
Comparison of the Orbital Properties of the Milky Way Globular Clusters from the Data of the Gaia DR2 and EDR3 Catalogs

A.T. Bajkova and V.V. Bobylev

*Central (Pulkovo) Astronomical Observatory, Russian Academy of Sciences,
Pulkovskoe shosse 65, St. Petersburg, 196140 Russia*

Abstract—We provide new values of the orbital parameters of 152 globular clusters, which are calculated using the new mean proper motions obtained from the Gaia EDR3 catalog data. The orbits were integrated 5 Gyr back in an axisymmetric three-component potential with a spherical bulge, disk component, and spherical dark halo in the Navarro–Frenk–White form, which we refined using the rotation curve of objects with large galactocentric distances up to 200 kpc. The obtained orbital parameters were compared with the orbital parameters of the same globular clusters calculated earlier in the same gravitational potential using proper motions from the Gaia DR2 catalog data. The objects whose orbits underwent significant changes were identified.

DOI: 10.1134/S1063772921090018

1 INTRODUCTION

Globular star clusters (GCs) are among the most interesting objects in our Galaxy. Studies of GCs provide understanding of the birth and evolution of the Galaxy, since they are the oldest stellar formations. Their age is almost equal to the age of the Universe. Approximately 170 Milky Way GCs are currently known. According to theoretical estimates, the number of GCs in the Milky Way can be around 200.

One of the methods of GC studies is to examine their orbital motion, which became possible thanks to high-accuracy measurements of their spatial velocities and positions from the Gaia spacecraft. The appearance of catalogs of mean proper motions based on the second DR2 release in combination with other astrometric data on GC radial velocities and positions made it possible to study the orbital motion of nearly all GCs known to date [1–3].

Among the astrometric data catalogs with proper motions from Gaia DR2, we would like to specifically mention Vasiliev’s (2019) catalog for 150 GCs [3], which allows the construction of the 6d phase space required for the calculation of orbits. We used this catalog to study the orbital properties of GCs. Thus, we developed a new method for separating GCs by subsystems of the Galaxy: bulge, thick disk, and halo [4]. The separation method is based on the bimodality we discovered in the GC distribution over the parameter L_Z/ecc , where L_Z is the Z component of the angular momentum and ecc is the orbital eccentricity. Due to this bimodality, GCs belonging to the disk, i.e., those that formed in the Galaxy itself, can

be easily distinguished from halo GCs of extragalactic origin using the probabilistic method described in detail in [4].

Massari et al. [5] give a classification of halo GCs that formed outside the Milky Way and ended up in our Galaxy as a result of accretion from dwarf galaxies (Sagittarius, Sausage, Sequoia [6]). A catalog of 152 GC orbits and their orbital parameters is presented by us in [7], as well as a modified classification by the Galaxy subsystems based on the obtained orbital properties of GCs. This classification is confirmed in this study as well.

The appearance of a new, more accurate version of the GC proper motions catalog [8] based on the Gaia EDR3 measurement data leads to a natural problem of refining the GC orbital parameters and identifying GCs whose orbital motion underwent the greatest changes. This is the scope of the present paper.

This study is structured as follows. The first section provides a brief description and justification of the adopted model of the gravitational potential in which the GC orbits are integrated; the equations of motion and the formulas for calculating the orbital parameters are also given. The second section describes the data and compares the mean proper motions and their uncertainties obtained from the data of the Gaia DR2 and EDR3 catalogs. The third section is dedicated to the discussion of the study results; a catalog of GC orbital parameters calculated from the Gaia EDR3 data is presented, and they are compared with the orbital parameters obtained from the Gaia DR2 catalog and published in [7]; the orbits for a number of GCs that have undergone the greatest changes are given. The main conclusions are drawn in the final section.

2 METHODS

2.1 Axisymmetric Galactic Potential Model

The axisymmetric gravitational potential of the Galaxy is represented as a sum of three components: central spherical bulge $\Phi_b(r(R, Z))$, disk $\Phi_d(r(R, Z))$, and a massive spherical dark-matter halo $\Phi_h(r(R, Z))$ [9, 10]:

$$\Phi(R, Z) = \Phi_b(r(R, Z)) + \Phi_d(r(R, Z)) + \Phi_h(r(R, Z)). \quad (1)$$

Here, we use a cylindrical coordinate system (R, ψ, Z) with the origin at the center of the Galaxy. In a rectangular Cartesian coordinate system (X, Y, Z) with the origin at the center of the Galaxy, the distance to the star (spherical radius) is $r^2 = X^2 + Y^2 + Z^2 = R^2 + Z^2$.

The bulge $\Phi_b(r(R, Z))$ and disk $\Phi_d(r(R, Z))$ potentials are expressed in the form proposed by Miyamoto and Nagai [11], and the halo component is represented according to Navarro et al. [12]. The specific values of the parameters of this model, provided that the potential is expressed in units of $100 \text{ km}^2/\text{s}^2$, distances in kpc, masses in units of the mass of the Galaxy, $M_{gal} = 2.325 \times 10^7 M_\odot$, and the gravitational constant $G = 1$, are given in the paper by Bajkova and Bobylev [9], where it is designated as model III.

It should be noted that the model of the galactic potential that we have adopted and denoted here, same as in [7], by NFWBB, has the parameters obtained by fitting them to the data on the circular velocities of ionized hydrogen clouds HI, maser sources, and various halo objects with large galactocentric distances R up to ~ 200 kpc from Bhattacharjee et al. [13] (see Fig. 1). In addition, the fitting of the parameters involved the constraints on the local dynamic density of matter $\rho_\odot = 0.1 M_\odot \text{ pc}^{-3}$ and the force acting perpendicular to the plane of the Galaxy $|K_{z=1.1}|/2\pi G = 77 M_\odot \text{ pc}^{-2}$ [14].

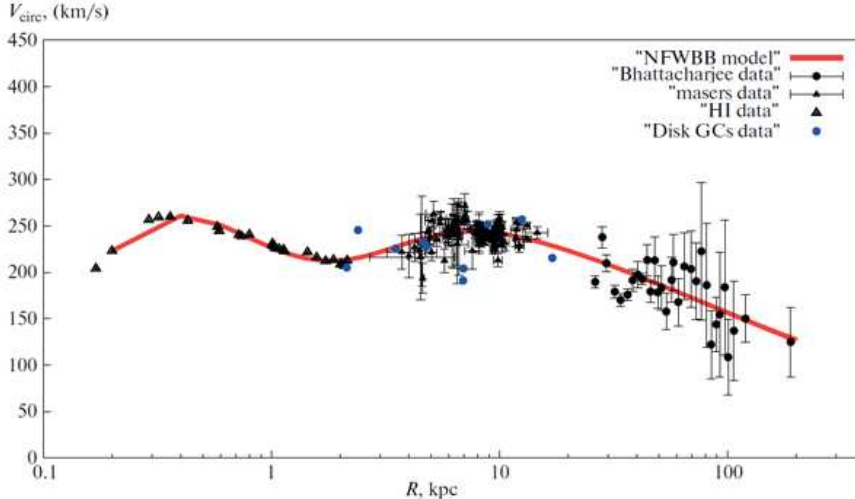


Figure 1: Rotation curve corresponding to the NFWBB model of the potential. The blue dots show the circular velocities of the disk GCs with orbital eccentricities ≤ 0.2 .

The rotation curve corresponding to the NFWBB model is shown in Fig. 1. We plotted this curve using the values $R_\odot = 8.3$ kpc for the galactocentric distance of the Sun and $V_\odot = 244$ km/s for the rotation's linear velocity of the local standard of rest around the Galaxy center, as it is taken in [13]. According to this model [9], the mass of the Galaxy $M_{G(R \leq 200 \text{ kpc})} = 0.75 \pm 0.19 \times 10^{12} M_\odot$. This value is in good agreement with modern independent estimates. For example, the lower estimate of the NFW halo mass obtained quite recently by Koppelman and Helmi [15] from the data on the velocities of runaway halo stars is $M_{G(R \leq 200 \text{ kpc})} = 0.67^{+0.30}_{-0.15} \times 10^{12} M_\odot$. Figure 1, in addition to the available data, also shows the circular velocities of the thick disk GCs with orbital eccentricities ≤ 0.2 (blue dots), which demonstrate good agreement with the data from maser sources at interval of galactocentric distances $2 < R < 20$ kpc.

The model of the gravitational potential of the Milky Way NFWBB appears to us the most realistic in comparison with other known models, since it is supported by data at large galactocentric distances, which is very important in integration of the orbits of distant globular clusters and clusters with a large apocentric distance; it also agrees well with modern estimates of the local parameters and independent estimates of the mass of the Galaxy [10], a thorough review of which was also recently given by Wang et al. [16].

2.2 Integration of the Orbits

The equation of motion of a test particle in an axisymmetric gravitational potential can be obtained from the Lagrangian of the system \mathcal{L} (see Appendix A in Irrgang et al. [14]):

$$\mathcal{L}(R, Z, \dot{R}, \dot{\psi}, \dot{Z}) = 0.5(\dot{R}^2 + (R\dot{\psi})^2 + \dot{Z}^2) - \Phi(R, Z). \quad (2)$$

Introducing canonical moments

$$\begin{aligned} p_R &= \partial\mathcal{L}/\partial\dot{R} = \dot{R}, \\ p_\psi &= \partial\mathcal{L}/\partial\dot{\psi} = R^2\dot{\psi}, \\ p_Z &= \partial\mathcal{L}/\partial\dot{Z} = \dot{Z}, \end{aligned} \quad (3)$$

we obtain the Lagrange equations as a system of six first-order differential equations:

$$\begin{aligned}
\dot{R} &= p_R, \\
\dot{\psi} &= p_\psi/R^2, \\
\dot{Z} &= p_Z, \\
\dot{p}_R &= -\partial\Phi(R, Z)/\partial R + p_\psi^2/R^3, \\
\dot{p}_\psi &= 0, \\
\dot{p}_Z &= -\partial\Phi(R, Z)/\partial Z.
\end{aligned} \tag{4}$$

To integrate Eqs. (4), we used our own integrator that implements the fourth-order Runge–Kutta algorithm.

The peculiar velocity of the Sun relative to the local standard of rest was considered equal to $(u_\odot, v_\odot, w_\odot) = (11.1, 12.2, 7.3) \pm (0.7, 0.5, 0.4) \text{ km s}^{-1}$ [17]. Here, we use heliocentric velocities in a moving Cartesian coordinate system with u velocity directed toward the galactic center, v in the direction of the Galaxy rotation, and w perpendicular to the plane of the Galaxy and directed to the north pole of the Galaxy.

Let the initial positions and spatial velocities of the test particle in the heliocentric coordinate system be $(x_o, y_o, z_o, u_o, v_o, w_o)$. The initial positions (X, Y, Z) and velocities (U, V, W) of the test particle in the Cartesian coordinates of the Galaxy are given by the formulas

$$\begin{aligned}
X &= R_\odot - x_o, Y = y_o, Z = z_o + h_\odot, \\
R &= \sqrt{X^2 + Y^2}, \\
U &= u_o + u_\odot, \\
V &= v_o + v_\odot + V_\odot, \\
W &= w_o + w_\odot,
\end{aligned} \tag{5}$$

where R_\odot and V_\odot are the galactocentric distance and linear velocity of rotation of the local standard of rest around the center of the Galaxy, and $h_\odot = 16 \text{ pc}$ [18] is the elevation of the Sun above the plane of the Galaxy.

In this study, we calculate the following orbital parameters of globular clusters: (1) the initial distance of the GC from the center of the Galaxy d_{GC} ; (2) radial velocity Π ; (3) circular velocity Θ ; (4) total 3D velocity V_{tot} ; (5) apocentric distance (*apo*) of the orbit; (6) pericentric distance (*peri*) of the orbit; (7) eccentricity (*ecc*) of the orbit; (8) angular momentum components; (9) the angle of orbital inclination θ ; (10) orbital period T_r ; and (11) total energy E .

The formulas for calculating all of the listed orbital parameters are given in [7]. The uncertainties of the orbital parameters were calculated by the Monte Carlo method using 100 iterations considering the uncertainties in the initial GC coordinates and velocities, as well as errors in the peculiar velocity of the Sun.

3 DATA

For the previously examined 152 globular clusters [7] with the data mainly from Vasiliev’s catalog [3], we took only the new values of mean proper motions and their uncertainties from the new catalog by Vasiliev and Baumgardt [8] obtained from the Gaia EDR3 catalog data. All other astrometric data (distances, radial velocities, coordinates) remained the same. Although the new catalog of Vasiliev and Baumgardt [8] also contains new, more

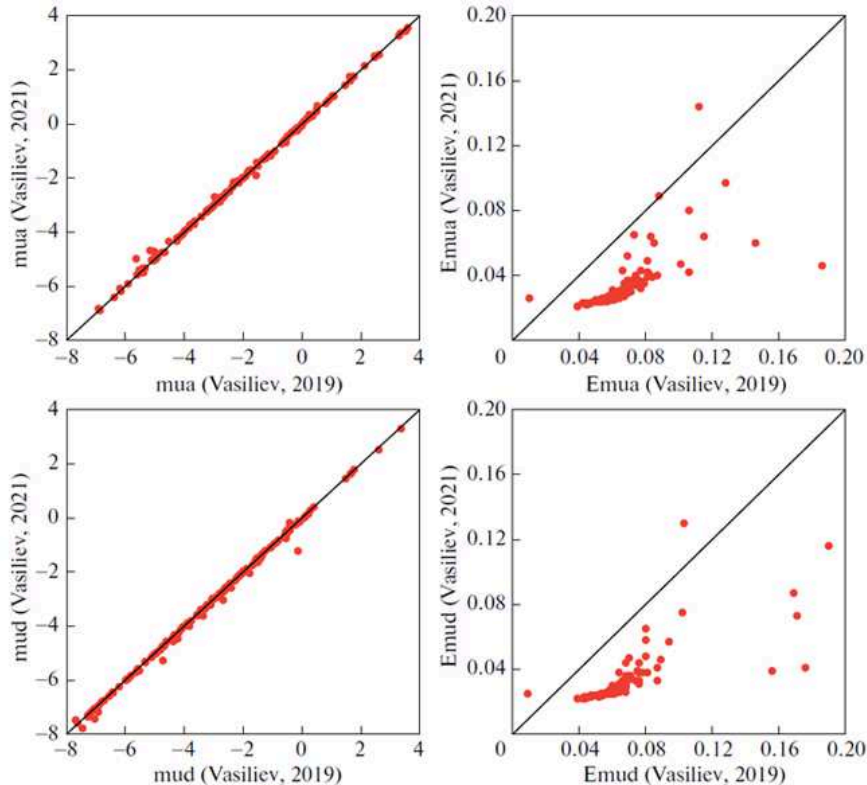


Figure 2: Comparison of the GC proper motions (by α , mua and δ , mud) and their uncertainties (Emua and Emud, respectively) from Vasiliev’s catalog [3] (Gaia DR2, horizontal axis) and Vasiliev and Baumgardt’s catalog [8] (Gaia EDR3, vertical axis). Each panel has a coincidence line.

accurate mean values of trigonometric parallaxes, their uncertainty remains rather large as compared to the distances found from the horizontal giant branch [19] in Vasiliev’s catalog [3].

In Fig. 2, we give a comparison of the mean proper motions from these two catalogs obtained from the Gaia DR2 and Gaia EDR3 measurements. As follows from the figure, the new proper motion values for a number of GCs differ markedly from the old values. At the same time, the accuracy of measuring the new proper motions has doubled on average.

4 RESULTS

Table 1 shows the orbital parameters of 152 GCs listed in Section 2.2, which are calculated for the new mean proper motions from EDR3 [8].

The values of the parameters obtained from the integration of the orbits 5 Gyr back are given for each GC. The columns show the initial GC distance from the center of the Galaxy d_{GC} ; radial velocity Π ; circular velocity Θ ; total 3D velocity V_{tot} ; apocentric distance (apo) of the orbit; pericentric distance (peri) of the orbit; eccentricity (ecc) of the orbit; orbital inclination angle θ ; orbital period T_r ; Z component of the angular momentum L_Z ; total energy E ; and subsystem in the Galaxy to which the object is assigned. The objects with the greatest changes in the orbital properties are marked with an asterisk.

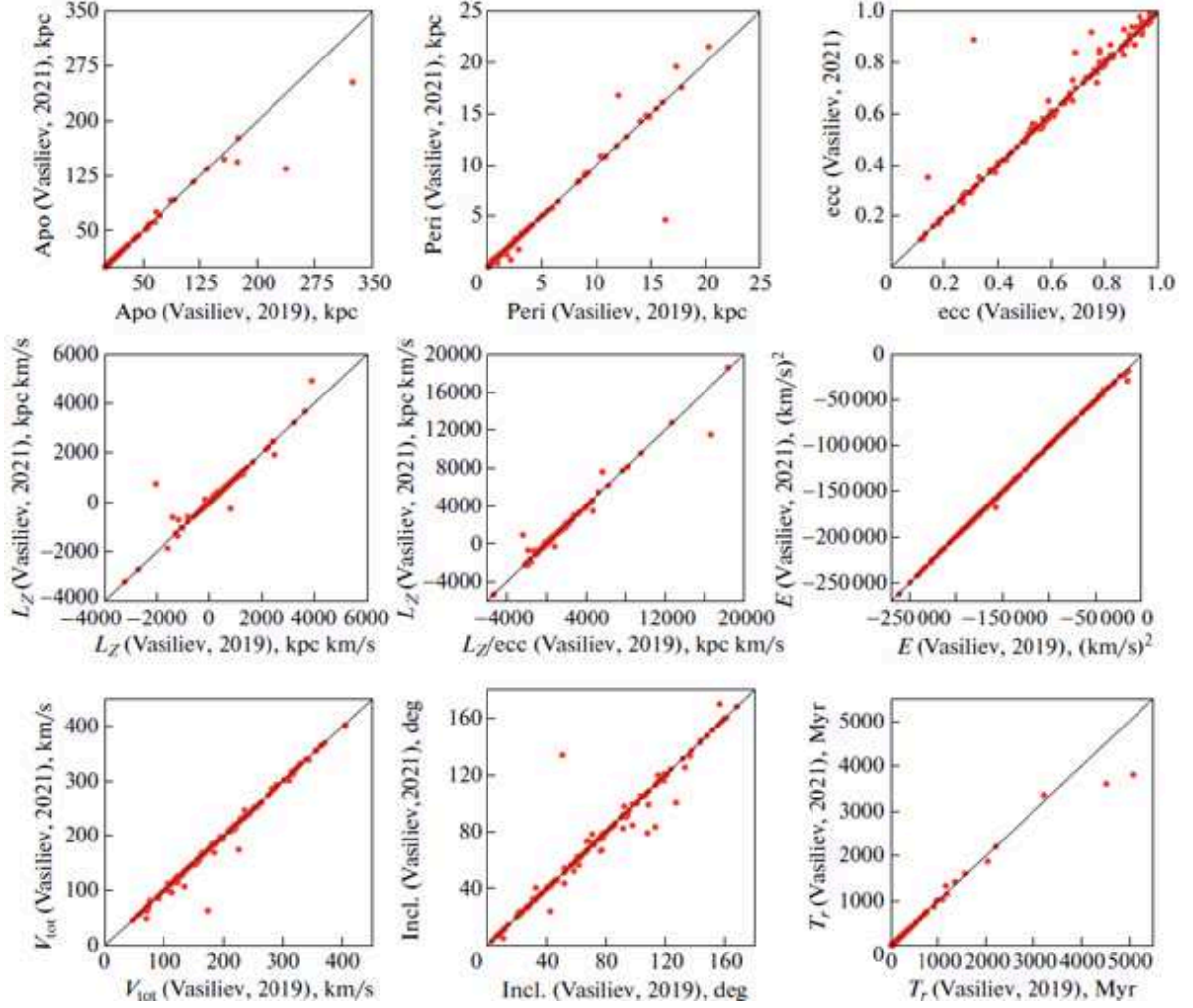


Figure 3: Comparison of the GC orbital parameters (apo , $peri$, ecc , L_z , l_z/ecc , E , V_{tot} , θ , T_r) obtained using Vasiliev's catalog (2019) [3] with mean proper motions from Gaia DR2 (horizontal axis) and Vasiliev and Baumgardt's catalog (2021) [8] with mean proper motions from Gaia EDR3 (vertical axis). Each panel has a diagonal coincidence line.

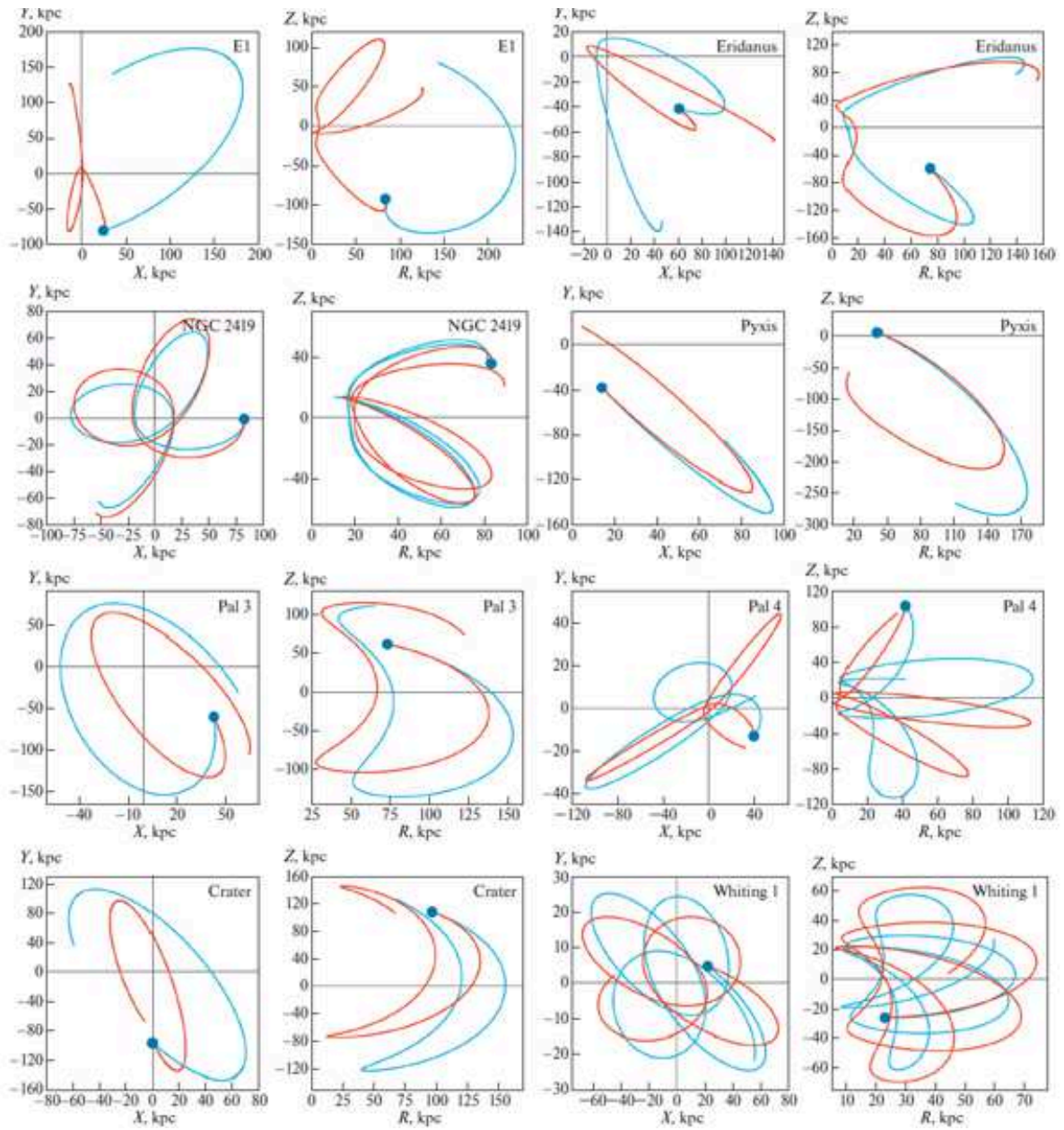


Figure 4: Orbits of very distant GCs. Blue color shows GC orbits with proper motions from Gaia DR2, red color from Gaia EDR3. The beginning of the orbit is marked with a blue circle.

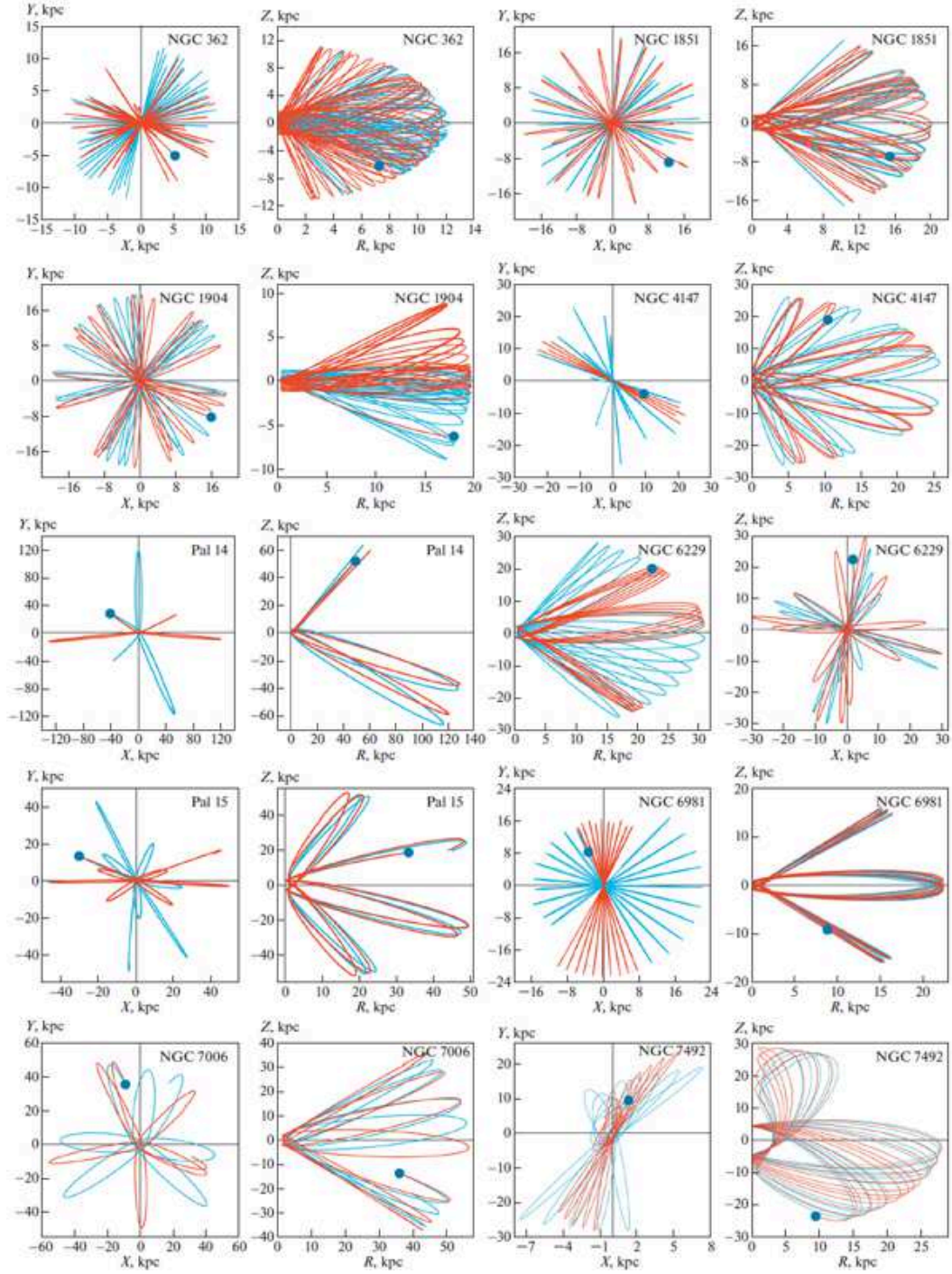


Figure 5: Strongly radially elongated GC orbits. Blue color shows GC orbits with proper motions from Gaia DR2, red color from Gaia EDR3. The beginning of the orbit is marked with a blue circle.

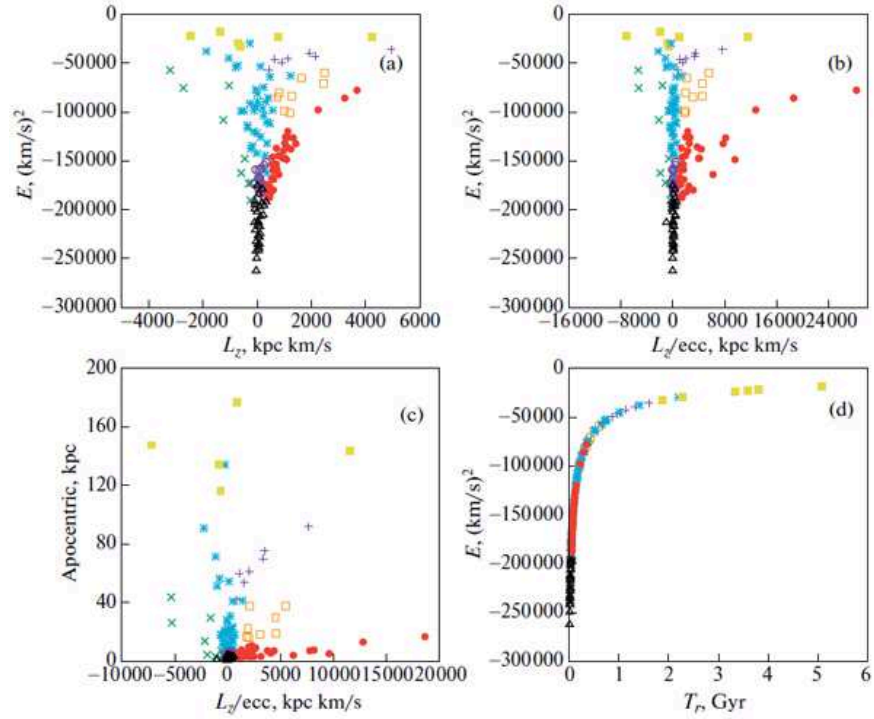


Figure 6: Two-dimensional diagrams (a) $L_Z - E$, (b) $L_Z/\text{ecc} - E$, (c) $L_Z/\text{ecc} - apo$, and (d) $T_r - E$. Different symbols indicate the belonging of the GC to different subsystems of the Galaxy: red circles—disk (D), black triangles—bulge (B), blue stars—Gaia- Enceladus (GE), orange squares—Helmi stream (H99), green crosses—Sequoia galaxy (Seq), purple crosses—Sagittarius dwarf galaxy (Sgr), yellow squares—unassociated high energy group (HE), purple open circles—unassociated low energy group (LE).

The column shows the belonging of the clusters to a subsystem of the Galaxy. The following designations of subsystems are adopted, similar to those in [5]: D is disk; B is bulge; GE is the Sausage galaxy, or Gaia–Enceladus; H99 is the Helmi stream; Seq is the Sequoia galaxy; Sgr is the Sagittarius dwarf galaxy; HE is the unassociated high energy group; and LE is the unassociated low energy group. The GCs were divided into subsystems of the bulge (B), thick disk (D), and halo in accordance with the algorithm we proposed [4]. The GC classification by halo subsystems (Seq, Sqr, GE, H99, HE, LE) was proposed by Massari et al. [5]. In [7], we modified the classification of Massari et al. in accordance with the orbital features of the GCs. Twenty-seven objects were modified. The analysis of the new orbital parameters kept this classification in force.

The GC orbital parameters calculated using the Gaia EDR3 mean proper motions were compared with the similar parameters [7] calculated from the Gaia DR2 data, which is shown in Fig. 3. As can be seen from the figures, a significant difference is observed for a number of GCs. We were able to identify 22 most prominent representatives.

As the analysis showed, the greatest change in the orbital parameters was experienced by very distant GCs, the measurement of proper motions associated with the greatest difficulties. Due to the increased accuracy of the data from the Gaia EDR3 catalog in comparison with the data from Gaia DR2, the proper motion values for distant objects have changed greatly. These objects are E1, Eridanus, Pyxis, Palomar 3, Palomar 4, and Crater belonging to the HE subsystem, and NGC 2419 and Whiting 1 belonging to Sqr. The orbits of these GCs in two projections (X, Y) and (R, Z) were plotted from the EDR3 and DR2 data are shown in Fig. 4 in red and blue, respectively. As can be seen from the figures, the greatest change in the orbit affected the most distant object E1.

Another class of objects that have undergone significant changes in orbital motion are GCs with highly elongated radial orbits. We have separately identified 10 most prominent representatives: NGC 362, NGC 1851, NGC 1904, NGC 4147, Palomar 14, NGC 6229, Palomar 15, NGC 6981, NGC 7006, and NGC 7492. They all belong to the GE subsystem. The orbits of these globular clusters are shown in Fig. 5. As can be seen from the figure, the orbits of three GCs underwent the most significant changes: Palomar 14, which is also among the most distant objects, Palomar 15, and NGC 6981.

It should be noted that the clusters E1, Eridanus, Pyxis, Palomar 3, Palomar 4, Crater, and Palomar 14 gave the largest deviations from the coincidence line in Fig. 3.

Four other GCs whose orbits have changed not so much but still noticeably are NGC 5946 and FSR 1735 of the LE subsystem, ESO 280–06 (GE), and the disk object NGC 6569.

Thus, the most distant objects and objects with orbits strongly elongated in the radial direction have undergone the greatest change in the orbital properties. All 22 GCs with significantly changed orbital properties are marked by an asterisk in the last column of Table 1. The orbits of the other GCs have changed very insignificantly, so the catalog of orbits presented in [7] can be used to study their dynamics.

Figure 6 shows two-dimensional diagrams (a) $L_Z - E$, (b) $L_Z/ecc - E$, (c) $L_Z/ecc - apo$, and (d) $T_r - E$. Diagrams (a), (b), and (c) are interesting in that they clearly show the fragmentation of the GC distribution over the subsystems of the Galaxy. Diagram (b) with the L_Z/ecc values plotted along the horizontal axis instead of L_Z in comparison with diagram (a) allows for a finer structuring of the distribution of the thick disk GCs (D). This is due to the fact that disk objects have relatively small values of eccentricity, which allows “spreading” them along the abscissa axis as a result of division by ecc . The fine structure of the disk object distribution is also clearly visible in diagram (c). Apparently, further study

of the structural distribution of GCs is of interest from the point of view of a more subtle classification of GCs.

The $T_r - E$ diagram (d) is interesting in that it represents an unambiguous relationship between the period and the total energy of objects in the Galaxy set only by the gravitational potential of the Galaxy. This dependence can be fairly accurately fitted by a hyperbolic function. Thus, for example, knowing the total energy of a GC, one can immediately estimate the period of the orbit without integrating it. Conversely, knowing the period of the orbit, one can estimate the total energy E of a GC.

5 CONCLUSIONS

The emergence of increasingly more accurate astrometric data on the coordinates and spatial velocities of globular clusters makes it possible to study their motion in three-dimensional space by integrating the orbits in the gravitational potential of the Galaxy.

Thanks to the Gaia DR2 data [1–3] on the proper motions of almost all globular clusters known to date, it became possible to study their kinematics and dynamics and classify GCs according to the subsystems of the Milky Way in order to identify objects that formed directly in the Galaxy or were brought from outside as a result of accretion from other (dwarf) galaxies around the Milky Way. The creation of the catalog of orbits and their parameters for more than 150 GCs [7] with known data on the 6d phase space required for the integration of the orbits provides highly informative material for further research.

The recent appearance of a new, more accurate version of the catalog of proper motions posed the task of specifying the orbital motion of the GCs, which was the subject of this study. As a result of using new, more accurate proper motions determined from the Gaia EDR3 data, we were able to identify 22 GCs whose orbital motion underwent a significant change. Those are NGC 362, Whiting 1, E1, Eridanus, NGC 1851, NGC 1904, NGC 2419, Pyxis, Palomar 3, Palomar 4, Crater, NGC 4147, NGC 5946, Palomar 14, NGC 6229, FSR 1735, Palomar 15, ESO 280–06, NGC 6569, NGC 6981, NGC 7006, and NGC 7492. The major part of this list are very distant GCs, as well as GCs with orbits strongly elongated toward the center of the Galaxy, belonging to the Gaia-Enceladus subsystem.

Thus, the main result of this study is the creation of a new catalog of orbital parameters of 152 GCs with proper motions from Gaia EDR3, indicating objects with significantly changed orbital properties in comparison with the catalog based on the proper motions from Gaia DR2.

ACKNOWLEDGMENTS

The authors are grateful to the anonymous reviewer for comments that have helped improve the article.

REFERENCES

1. A. Helmi, F. van Leeuwen, P. J. McMillan, D. Massari, et al., *Astron. Astrophys.* 616, A12 (2018).
2. H. Baumgardt, M. Hilker, A. Sollima, and A. Bellini, *Mon. Not. R. Astron. Soc.* 482, 5138 (2019).
3. E. Vasiliev, *Mon. Not. R. Astron. Soc.* 484, 2832 (2019).

4. A. T. Bajkova, G. Carraro, V. I. Korchagin, N. O. Budanova, and V. V. Bobylev, *Astrophys. J.* 895, 69 (2020).
5. D. Massari, H. H. Koppelman and A. Helmi, *Astron. Astrophys.* 630, L4 (2019).
6. G. C. Myeong, E. Vasiliev, G. Iorio, N. W. Evans, and V. Belokurov, *Mon. Not. R. Astron. Soc.* 488, 1235 (2019).
7. A. T. Bajkova and V.V. Bobylev, *Res. Astron. Astrophys.* **21**, 173 (2021).
8. E. Vasiliev and H. Baumgardt, arXiv: 2102.09568 [astro-ph.GA] (2021).
9. A. T. Bajkova and V. V. Bobylev, *Astron. Lett.* 42, 567 (2016).
10. A. T. Bajkova and V. V. Bobylev, *Open Astron.* 26, 72 (2017).
11. M. Miyamoto and R. Nagai, *Publ. Astron. Soc. Jpn.* 27, 533 (1975).
12. J. F. Navarro, C. S. Frenk, and S. D. M. White, *Astrophys. J.* 490, 493 (1997).
13. P. Bhattacharjee, S. Chaudhury, and S. Kundu, *Astrophys. J.* 785, 63 (2014).
14. A. Irrgang, B. Wilcox, E. Tucker, and L. Schiefelbein, *Astron. Astrophys.* 549, A137 (2013).
15. H. H. Koppelman and A. Helmi, arXiv: 2006.16283 [astro-ph.GA] (2020).
16. W. Wang, J. Han, M. Cautun, Z. Li, and M. Ishigaki, *Sci. China Phys. Mech. Astron.* 63, 109801 (2020).
17. R. Schönrich, J. Binney, and W. Dehnen, *Mon. Not. R. Astron. Soc.* 403, 1829 (2010).
18. V. V. Bobylev and A. T. Bajkova, *Astron. Lett.* 42, 1 (2016).
19. W. Harris, arXiv: 1012.3224 [astro-ph.GA] (2010).

Table 1. Orbital properties of GCs

Name	d_{GC} [kpc]	Π [km/s]	Θ [km/s]	V_{tot} [km/s]	apo [kpc]	peri [kpc]	ecc	incl. θ [deg]	T_r [Gyr]	L_Z [kpc km/s]	E [km ² /s ²]	Gal. Sub- syst	
NGC 104	7.6	6 ⁺⁶ ₋₅	191 ⁺⁴ ₋₄	197 ⁺⁴ ₋₄	7.7 ^{+0.1} _{-0.1}	5.52 ^{+0.22} _{-0.19}	0.16 ^{+0.02} _{-0.01}	28 ⁺¹ ₋₁	116 ⁺³ ₋₃	1325 ⁺³⁴ ₋₃₆	-126360 ⁺¹²³⁷ ₋₁₀₇₁	D	
NGC 288	12.2	4 ⁺¹ ₋₁	-42 ⁺¹⁷ ₋₁₃	66 ⁺⁹ ₋₉	12.4 ^{+0.3} _{-0.4}	1.33 ^{+0.45} _{-0.33}	0.81 ^{+0.07} _{-0.06}	121 ⁺⁴ ₋₄	142 ⁺⁵ ₋₅	-349 ⁺¹⁴² ₋₁₀₅	-116316 ⁺¹⁶⁵⁴ ₋₁₇₈₀	GE	
NGC362	9.5	126 ⁺⁵ ₋₉	-2 ⁺⁷ ₋₁₁	144 ⁺⁵ ₋₈	11.7 ^{+0.5} _{-0.2}	0.08 ^{+0.00} _{-0.00}	0.99 ^{+0.04} _{-0.04}	93 ⁺¹⁸ ₋₁₀	126 ⁺³ ₋₃	-12 ⁺⁷⁹ ₋₇₉	-121469 ⁺¹⁰⁶⁴ ₋₁₆₆₄	GE	*
Whiting 1	34.7	-232 ⁺¹¹ ₋₁₆	85 ⁺¹³ ₋₁₅	247 ⁺¹⁶ ₋₁₀	75.4 ^{+17.0} _{-9.0}	21.56 ^{+1.86} _{-1.78}	0.56 ^{+0.05} _{-0.03}	74 ⁺³ ₋₂	1328 ⁺³³⁹ ₋₁₇₇	1927 ⁺³⁰⁵ ₋₃₆₂	-39308 ⁺⁴⁴⁵⁴ ₋₃₀₁₁	Sgr	*
NGC 1261	18.2	-98 ⁺⁵ ₋₈	-21 ⁺⁷ ₋₆	121 ⁺⁷ ₋₅	21.2 ^{+0.8} _{-0.6}	0.81 ^{+0.35} _{-0.14}	0.93 ^{+0.01} _{-0.03}	120 ⁺⁷ ₋₁₁	246 ⁺¹⁰ ₋₉	-273 ⁺⁹⁵ ₋₈₂	-91128 ⁺¹⁹⁰⁸ ₋₁₃₃₅	GE	
Pal 1	17.4	43 ⁺⁵ ₋₆	215 ⁺² ₋₂	221 ⁺² ₋₂	19.2 ^{+0.5} _{-0.6}	14.83 ^{+0.47} _{-0.44}	0.13 ^{+0.02} _{-0.02}	15 ⁺¹ ₋₀	356 ⁺¹⁰ ₋₁₀	3677 ⁺⁶⁹ ₋₈₂	-77542 ⁺⁹⁴⁶ ₋₁₀₉₅	D	
E 1	124.7	-16 ⁺⁵⁸ ₋₃₆	-8 ⁺⁵² ₋₅₆	63 ⁺⁷⁸ ₋₀	134.5 ^{+64.9} _{-24.9}	8.03 ^{+63.43} _{-0.00}	0.89 ^{+0.00} _{-0.49}	101 ⁺²² ₋₃₂	2280 ⁺¹⁹⁹³ ₋₁₅₀	-706 ⁺⁴²⁶³ ₋₄₆₄₆	-28995 ⁺⁸³⁰⁶ ₋₄₅₃	HE	*
Eridanus	95.2	-74 ⁺¹⁸ ₋₁₄	10 ⁺¹⁸ ₋₁₂	166 ⁺¹² ₋₁₉	176.7 ^{+20.3} _{-27.8}	16.77 ^{+5.66} _{-4.38}	0.83 ^{+0.03} _{-0.06}	84 ⁺⁷ ₋₁₃	3348 ⁺⁵²⁴ ₋₆₄₁	753 ⁺¹³⁵⁶ ₋₈₇₄	-23513 ⁺¹⁸³⁵ ₋₂₉₅₄	HE	*
Pal 2	35.3	-107 ⁺³ ₋₄	13 ⁺⁹ ₋₁₃	108 ⁺⁴ ₋₂	40.9 ^{+1.8} _{-1.8}	0.84 ^{+0.23} _{-0.46}	0.96 ^{+0.02} _{-0.03}	24 ⁺⁶⁶ ₋₂₁	506 ⁺²⁶ ₋₂₄	467 ⁺³²⁰ ₋₄₄₆	-63898 ⁺¹⁵⁹⁸ ₋₁₇₀₄	GE	
NGC 1851	16.9	104 ⁺² ₋₃	-5 ⁺⁴ ₋₄	132 ⁺⁴ ₋₃	20.1 ^{+0.4} _{-0.4}	0.14 ^{+0.00} _{-0.00}	0.99 ^{+0.00} _{-0.03}	98 ⁺⁷ ₋₇	228 ⁺⁷ ₋₄	-76 ⁺⁶⁶ ₋₆₀	-94253 ⁺¹⁰⁶⁹ ₋₁₀₇₈	GE	*
NGC 1904	19.0	45 ⁺⁴ ₋₄	11 ⁺⁵ ₋₆	47 ⁺⁴ ₋₃	19.7 ^{+0.2} _{-0.6}	0.35 ^{+0.25} _{-0.12}	0.97 ^{+0.01} _{-0.03}	62 ⁺¹⁶ ₋₁₄	218 ⁺⁸ ₋₁₀	192 ⁺⁹⁸ ₋₁₁₅	-96229 ⁺¹¹⁰⁸ ₋₉₇₄	GE	*
NGC 2298	16.0	-92 ⁺⁷ ₋₆	-31 ⁺⁶ ₋₆	124 ⁺⁷ ₋₆	18.0 ^{+0.4} _{-0.4}	1.25 ^{+0.34} _{-0.15}	0.87 ^{+0.01} _{-0.03}	117 ⁺⁵ ₋₅	208 ⁺⁶ ₋₆	-494 ⁺⁹⁴ ₋₉₅	-98729 ⁺¹³⁰⁰ ₋₁₁₇₁	GE	
NGC 2419	90.2	-7 ⁺⁶ ₋₅	59 ⁺¹³ ₋₁₃	80 ⁺¹⁴ ₋₁₀	91.9 ^{+3.5} _{-3.2}	19.60 ^{+9.62} _{-5.54}	0.65 ^{+0.07} _{-0.12}	44 ⁺⁸ ₋₆	1600 ⁺²¹⁹ ₋₈₁₅	4937 ⁺¹¹²⁵ ₋₁₁₃₂	-35478 ⁺¹⁵³⁷ ₋₁₁₉₀	Sgr	*
Pyxis	41.5	-246 ⁺⁴ ₋₄	-34 ⁺¹⁰ ₋₁₀	301 ⁺⁴ ₋₆	252.7 ^{+39.9} _{-43.8}	41.69 ^{+1.53} _{-20.48}	0.72 ^{+0.12} _{-0.00}	100 ⁺³ ₋₃	5084 ⁺¹²⁴⁷ ₋₁₃₉₃	-1382 ⁺⁴⁷⁹ ₋₄₅₈	-18116 ⁺²¹³⁹ ₋₁₉₇₀	HE	*
NGC 2808	11.3	-157 ⁺² ₋₁	41 ⁺⁴ ₋₄	165 ⁺¹ ₋₁	14.4 ^{+0.5} _{-0.5}	1.01 ^{+0.09} _{-0.07}	0.87 ^{+0.01} _{-0.02}	10 ⁺¹ ₋₁	158 ⁺⁶ ₋₆	460 ⁺³⁴ ₋₃₀	-111826 ⁺¹⁸⁸⁵ ₋₁₇₆₄	GE	
E 3	9.3	44 ⁺¹² ₋₁₁	252 ⁺⁸ ₋₉	275 ⁺⁹ ₋₉	13.1 ^{+1.3} _{-1.1}	9.18 ^{+0.30} _{-0.31}	0.18 ^{+0.04} _{-0.04}	29 ⁺¹ ₋₁	224 ⁺¹⁴ ₋₁₂	2244 ⁺¹⁰⁷ ₋₁₁₂	-97762 ⁺³¹¹³ ₋₂₈₅₈	D	
Pal 3	95.9	-146 ⁺¹⁵ ₋₂₀	58 ⁺²⁷ ₋₃₀	169 ⁺²² ₋₁₆	144.0 ^{+59.4} _{-22.6}	66.53 ^{+14.11} _{-15.05}	0.37 ^{+0.12} _{-0.03}	73 ⁺⁸ ₋₇	3602 ⁺¹²⁵⁹ ₋₆₈₁	4236 ⁺²⁰²⁹ ₋₂₂₁₅	-22836 ⁺⁴⁰⁰⁴ ₋₂₆₉₈	HE	*
NGC 3201	9.1	-114 ⁺⁸ ₋₁₀	-301 ⁺⁶ ₋₅	356 ⁺⁷ ₋₆	26.4 ^{+2.0} _{-1.8}	8.39 ^{+0.17} _{-0.23}	0.52 ^{+0.02} _{-0.03}	152 ⁺¹ ₋₁	376 ⁺²⁵ ₋₂₆	-2727 ⁺⁸³ ₋₇₀	-75366 ⁺²⁵⁰⁴ ₋₂₅₁₇	Seq	
Pal 4	111.4	2 ⁺¹⁹ ₋₁₉	-15 ⁺²⁷ ₋₁₇	49 ⁺¹⁷ ₋₁₅	116.4 ^{+0.0} _{-9.2}	4.61 ^{+9.33} _{-2.03}	0.92 ^{+0.03} _{-0.14}	105 ⁺⁴ ₋₄	1870 ⁺⁰ ₋₈₀₇	-615 ⁺¹¹⁰⁷ ₋₆₅₀	-32274 ⁺¹⁵⁷³ ₋₅₅₀	HE	*
Crater	144.8	-89 ⁺⁷⁶ ₋₅₄	-25 ⁺⁶⁴ ₋₁₁₇	107 ⁺¹⁰¹ ₋₁₅	147.7 ^{+426.9} _{-76.0}	71.90 ^{+84.24} _{-9.28}	0.35 ^{+0.33} _{-0.11}	99 ⁺²⁸ ₋₁₉	3806 ⁺¹⁸²³ ₋₃₃₆₃	-2469 ⁺⁶³⁵² ₋₁₁₃₉₃	-22149 ⁺¹⁷⁰⁶⁹ ₋₂₂₁₅	HE	*
NGC 4147	21.5	47 ⁺⁶ ₋₅	-0 ⁺¹² ₋₁₃	136 ⁺⁴ ₋₃	26.4 ^{+1.1} _{-1.1}	0.39 ^{+0.55} _{-0.00}	0.97 ^{+0.00} _{-0.04}	91 ⁺¹⁵ ₋₁₂	314 ⁺¹⁵ ₋₁₄	-4 ⁺¹²⁵ ₋₁₃₀	-81056 ⁺¹⁷⁵⁵ ₋₁₈₇₆	GE	*
NGC 4372	7.3	17 ⁺⁷ ₋₈	133 ⁺⁷ ₋₇	149 ⁺⁷ ₋₇	7.3 ^{+0.3} _{-0.1}	3.00 ^{+0.24} _{-0.24}	0.42 ^{+0.03} _{-0.03}	28 ⁺¹ ₋₂	98 ⁺³ ₋₃	965 ⁺⁶¹ ₋₅₄	-139619 ⁺²¹³⁹ ₋₁₇₆₈	D	
Rup 106	18.5	-243 ⁺³ ₋₅	91 ⁺⁸ ₋₁₀	261 ⁺⁵ ₋₃	38.0 ^{+2.2} _{-2.1}	4.65 ^{+0.51} _{-0.36}	0.78 ^{+0.02} _{-0.02}	46 ⁺⁴ ₋₃	498 ⁺³⁴ ₋₃₂	1627 ⁺¹⁶⁷ ₋₂₀₃	-64947 ⁺²¹²¹ ₋₂₂₂₉	H99	
NGC 4590	10.3	-169 ⁺⁹ ₋₁₀	294 ⁺⁸ ₋₁₀	339 ⁺⁴ ₋₅	30.0 ^{+1.7} _{-1.5}	8.89 ^{+0.29} _{-0.28}	0.54 ^{+0.02} _{-0.01}	41 ⁺² ₋₁	430 ⁺²⁸ ₋₂₂	2454 ⁺⁹⁵ ₋₉₉	-70313 ⁺²⁰³⁹ ₋₁₉₀₅	H99	
NGC 4833	7.2	105 ⁺⁸ ₋₁₀	40 ⁺⁹ ₋₁₁	120 ⁺⁹ ₋₁₁	8.1 ^{+0.3} _{-0.3}	0.74 ^{+0.14} _{-0.20}	0.83 ^{+0.04} _{-0.02}	37 ⁺¹⁰ ₋₆	86 ⁺³ ₋₃	288 ⁺⁶⁵ ₋₈₃	-144343 ⁺²⁰⁵² ₋₂₁₄₄	GE	
NGC 5024	18.5	-95 ⁺³ ₋₄	143 ⁺⁴ ₋₆	186 ⁺⁶ ₋₆	22.4 ^{+1.0} _{-1.0}	9.11 ^{+0.51} _{-0.61}	0.42 ^{+0.01} _{-0.01}	74 ⁺¹ ₋₁	336 ⁺¹⁶ ₋₁₉	810 ⁺²⁹ ₋₃₉	-79888 ⁺¹⁸⁰⁵ ₋₂₂₀	H99	
NGC 5053	17.9	-91 ⁺⁴ ₋₃	137 ⁺⁶ ₋₆	168 ⁺⁵ ₋₆	18.0 ^{+0.9} _{-0.7}	10.87 ^{+0.97} _{-0.63}	0.25 ^{+0.02} _{-0.04}	76 ⁺¹ ₋₁	304 ⁺¹⁸ ₋₁₅	747 ⁺⁴³ ₋₃₉	-84546 ⁺²⁴¹⁶ ₋₂₀₂₀	H99	
NGC 5139	6.6	-70 ⁺⁴ ₋₄	-72 ⁺⁴ ₋₅	128 ⁺⁶ ₋₄	7.4 ^{+0.0} _{-0.3}	1.13 ^{+0.16} _{-0.07}	0.74 ^{+0.01} _{-0.04}	137 ⁺³ ₋₄	80 ⁺⁴ ₋₁	-463 ⁺³¹ ₋₃₄	-147822 ⁺¹⁶⁹³ ₋₁₅₂₁	Seq	
NGC 5272	12.2	-39 ⁺⁴ ₋₄	142 ⁺⁶ ₋₅	199 ⁺⁴ ₋₄	15.9 ^{+0.7} _{-0.6}	5.14 ^{+0.48} _{-0.21}	0.51 ^{+0.01} _{-0.03}	57 ⁺¹ ₋₁	210 ⁺¹³ ₋₇	987 ⁺⁴⁴ ₋₃₉	-98373 ⁺²¹⁴⁷ ₋₂₀₀₈	H99	
NGC 5286	8.9	-219 ⁺² ₋₂	-43 ⁺⁸ ₋₈	223 ⁺¹ ₋₁	13.7 ^{+0.6} _{-0.7}	0.80 ^{+0.20} _{-0.12}	0.89 ^{+0.01} _{-0.03}	124 ⁺⁴ ₋₅	152 ⁺⁸ ₋₇	-372 ⁺⁶⁹ ₋₆₈	-113576 ⁺²¹⁸⁸ ₋₃₇₄₅	H99	
NGC 5466	16.4	169 ⁺¹³ ₋₁₇	-137 ⁺¹⁵ ₋₁₀	313 ⁺³ ₋₁₀	51.3 ^{+5.3} _{-5.3}	5.76 ^{+0.66} _{-0.62}	0.80 ^{+0.01} _{-0.02}	108 ⁺² ₋₂	712 ⁺⁸⁹ ₋₉₆	-795 ⁺⁹¹ ₋₉₁	-54156 ⁺³⁰⁹⁹ ₋₃₆₁₀	GE	
NGC 5634	21.1	-47 ⁺⁸ ₋₈	34 ⁺¹⁰ ₋₁₂	63 ⁺⁵ ₋₂	21.6 ^{+0.9} _{-1.0}	2.05 ^{+0.36} _{-0.23}	0.83 ^{+0.01} _{-0.03}	72 ⁺⁶ ₋₄	256 ⁺¹⁴ ₋₁₁	303 ⁺⁸⁸ ₋₁₀₄	-89241 ⁺²⁰²⁵ ₋₂₀₄₂	GE	
NGC 5694	29.3	-182 ⁺⁶ ₋₅	-45 ⁺¹¹ ₋₁₁	254 ⁺⁷ ₋₇	71.5 ^{+5.4} _{-4.8}	2.81 ^{+11.27} _{-2.36}	0.92 ^{+0.08} _{-0.20}	133 ⁺⁴ ₋₇	1012 ⁺²⁸ ₋₉₁	-1058 ⁺²⁷⁹ ₋₂₉₆	-44810 ⁺²¹⁰⁹ ₋₂₀₅₅	GE	
IC 4499	15.6	-243 ⁺³ ₋₂	-73 ⁺⁸ ₋₈	261 ⁺² ₋₂	29.7 ^{+1.6} _{-1.8}	6.38 ^{+0.52} _{-0.20}	0.65 ^{+0.01} _{-0.03}	113 ⁺² ₋₂	402 ⁺²³ ₋₂₅	-1042 ⁺¹¹⁸ ₋₁₁₆	-72691 ⁺¹⁹⁹⁴ ₋₂₃₅₀	Seq	
NGC 5824	25.7	-41 ⁺⁹ ₋₁₁	109 ⁺¹² ₋₁₂	216 ⁺¹⁰ ₋₈	37.6 ^{+3.2} _{-2.2}	14.26 ^{+1.76} _{-1.73}	0.45 ^{+0.05} _{-0.04}	58 ⁺³ ₋₂	602 ⁺⁶³ ₋₄₆	2464 ⁺²⁹⁷ ₋₂₉₈	-59518 ⁺²⁸⁹² ₋₂₄₂₃	H99	
Pal 5	18.4	-53 ⁺¹ ₋₁	161 ⁺²² ₋₁₉	170 ⁺²² ₋₁₇	18.9 ^{+1.1} _{-0.6}	10.77 ^{+2.65} _{-1.74}	0.27 ^{+0.08} _{-0.09}	66 ⁺³ ₋₄	310 ⁺⁴² ₋₂₆	1262 ⁺²³⁰ ₋₁₇₅	-83186 ⁺⁴⁷⁷⁶ ₋₂₉₉₄	H99	
NGC 5897	7.3	86 ⁺¹⁸ ₋₁₅	96 ⁺¹⁵ ₋₁₂	158 ⁺¹⁴ ₋₁₂	8.7 ^{+0.3} _{-0.3}	1.89 ^{+0.43} _{-0.35}	0.64 ^{+0.06} _{-0.05}	61 ⁺⁴ ₋₃	106 ⁺⁷ ₋₅	359 ⁺⁸³ ₋₇₈	-131869 ⁺³⁴⁵⁴ ₋₂₂₈₉	GE	
NGC 5904	6.3	-291 ⁺¹⁴ ₋₁₀	126 ⁺¹⁰ ₋₈	365 ⁺¹¹ ₋₁₃	23.4 ^{+2.5} _{-2.6}	2.27 ^{+0.40} _{-0.08}	0.82 ^{+0.01} _{-0.03}	72 ⁺² ₋₂	288 ⁺³³ ₋₃₄	401 ⁺³² ₋₄₁	-85416 ⁺⁴³⁰⁵ ₋₄₈₉₂	GE	

Name	d_{GC} [kpc]	Π [km/s]	Θ [km/s]	V_{tot} [km/s]	apo [kpc]	peri [kpc]	ecc	incl. θ [deg]	T_r [Gyr]	L_Z [kpc km/s]	E [km ² /s ²]	Galactic Sub- system	
NGC 5927	4.7	-39 ⁺¹⁵ ₋₁₅	233 ⁺⁵ ₋₈	236 ⁺⁶ ₋₈	5.2 ^{+0.3} _{-0.3}	4.17 ^{+0.28} _{-0.29}	0.11 ^{+0.05} _{-0.03}	9 ⁺¹ ₋₁	82 ⁺⁵ ₋₄	1077 ⁺⁶² ₋₆₁	-148646 ⁺³⁰³¹ ₋₂₈₄₈	D	
NGC 5946	5.8	36 ⁺¹³ ₋₉	25 ⁺⁸ ₋₇	115 ⁺⁸ ₋₄	5.9 ^{+0.3} _{-0.2}	0.35 ^{+0.19} _{-0.05}	0.89 ^{+0.01} _{-0.05}	76 ⁺⁴ ₋₄	66 ⁺³ ₋₄	145 ⁺⁴⁹ ₋₄₂	-158142 ⁺²⁸⁷² ₋₂₁₅₄	LE	*
ESO 224-8	12.6	-44 ⁺²² ₋₂₂	257 ⁺¹⁷ ₋₁₉	261 ⁺¹⁷ ₋₁₇	16.8 ^{+3.0} _{-2.4}	11.84 ^{+0.60} _{-1.30}	0.17 ^{+0.08} _{-0.04}	7 ⁺¹ ₋₀	290 ⁺⁴⁰ ₋₄₀	3226 ⁺²³⁸ ₋₃₃₃	-85573 ⁺⁵⁰¹⁶ ₋₆₁₀₃	D	
NGC 5986	4.7	61 ⁺¹⁵ ₋₁₂	23 ⁺⁷ ₋₉	66 ⁺¹⁴ ₋₁₀	5.5 ^{+0.1} _{-0.6}	0.16 ^{+0.11} _{-0.05}	0.94 ^{+0.02} _{-0.04}	65 ⁺¹⁰ ₋₆	56 ⁺² ₋₄	94 ⁺³⁰ ₋₃₉	-168587 ⁺²⁰⁹³ ₋₂₇₇₇	LE	
FSR 1716	4.8	87 ⁺²² ₋₂₈	228 ⁺⁹ ₋₁₄	286 ⁺⁷ ₋₁₂	7.2 ^{+0.5} _{-0.7}	3.96 ^{+0.37} _{-0.38}	0.29 ^{+0.06} _{-0.07}	33 ⁺² ₋₂	108 ⁺⁶ ₋₆	1089 ⁺⁶² ₋₈₃	-135629 ⁺³¹³² ₋₄₃₆₁	D	
Pal 14	71.4	123 ⁺¹¹ ₋₁₁	-6 ⁺¹⁸ ₋₉	177 ⁺¹² ₋₁₂	134.2 ^{+9.8} _{-12.9}	0.73 ^{+0.00} _{-0.02}	0.99 ^{+0.03} _{-0.03}	134 ⁺⁰ ₋₈₄	2200 ⁺²¹⁸ ₋₂₆₃	-273 ⁺⁹⁰⁷ ₋₂₈₂	-29451 ⁺¹⁴¹² ₋₂₀₅₉	GE	*
BH 184	4.4	41 ⁺¹⁴ ₋₁₇	121 ⁺⁷ ₋₈	156 ⁺⁷ ₋₇	4.7 ^{+0.2} _{-0.2}	1.69 ^{+0.15} _{-0.15}	0.47 ^{+0.04} _{-0.03}	36 ⁺² ₋₂	58 ⁺³ ₋₂	532 ⁺³⁷ ₋₃₇	-168541 ⁺²⁷⁸⁸ ₋₂₃₁₇	D	
NGC 6093	3.7	33 ⁺⁸ ₋₉	16 ⁺¹³ ₋₅	71 ⁺⁸ ₋₅	4.8 ^{+0.0} _{-0.7}	0.06 ^{+0.38} _{-0.00}	0.98 ^{+0.00} _{-0.17}	83 ⁺⁴ ₋₆	44 ⁺³ ₋₂	25 ⁺²⁹ ₋₁₇	-176940 ⁺²⁸¹⁵ ₋₁₅₇₆	LE	
NGC 6121	6.3	-52 ⁺² ₋₂	9 ⁺¹¹ ₋₁₁	54 ⁺⁴ ₋₂	6.5 ^{+0.1} _{-0.1}	0.12 ^{+0.10} _{-0.03}	0.96 ^{+0.01} _{-0.03}	21 ⁺⁷⁶ ₋₃₁	68 ⁺² ₋₁	58 ⁺⁶⁹ ₋₇₀	-159029 ⁺¹¹⁴⁴ ₋₉₁₀	LE	
NGC 6101	11.1	-12 ⁺¹⁸ ₋₁₈	-312 ⁺³ ₋₄	369 ⁺³ ₋₄	43.7 ^{+3.7} _{-3.6}	10.85 ^{+0.51} _{-0.51}	0.60 ^{+0.02} _{-0.01}	143 ⁺¹ ₋₁	652 ⁺⁶¹ ₋₆₀	-3217 ⁺¹⁶³ ₋₁₅₂	-57030 ⁺²⁶⁰⁹ ₋₂₈₃₂	Seq	
NGC 6144	2.7	-70 ⁺⁵⁶ ₋₅₄	-197 ⁺³⁴ ₋₁₄	213 ⁺² ₋₇	3.3 ^{+0.2} _{-0.1}	2.13 ^{+0.11} _{-0.20}	0.21 ^{+0.06} _{-0.02}	114 ⁺⁴ ₋₄	40 ⁺¹¹ ₋₁₀	-240 ⁺³⁸ ₋₃₁	-172490 ⁺²⁵⁸⁹ ₋₁₉₀₃	Seq	
NGC 6139	3.5	-1 ⁺¹¹ ₋₁₉	74 ⁺⁶ ₋₇	151 ⁺⁷ ₋₆	3.6 ^{+0.3} _{-0.1}	1.01 ^{+0.20} _{-0.08}	0.56 ^{+0.03} _{-0.05}	61 ⁺³ ₋₃	50 ⁺³ ₋₂	244 ⁺²⁵ ₋₂₅	-177317 ⁺¹⁹⁷² ₋₁₉₇₂	LE	
Terzan 3	2.5	-60 ⁺³⁸ ₋₃₆	205 ⁺⁸ ₋₁₆	234 ⁺⁷ ₋₇	3.2 ^{+0.3} _{-0.1}	2.20 ^{+0.22} _{-0.29}	0.18 ^{+0.08} _{-0.05}	42 ⁺⁴ ₋₄	44 ⁺⁵ ₋₃	439 ⁺⁴⁸ ₋₄₉	-175727 ⁺³²⁹⁷ ₋₂₄₀₁	D	
NGC 6171	3.5	-4 ⁺³ ₋₂	77 ⁺⁸ ₋₈	101 ⁺⁸ ₋₇	3.8 ^{+0.2} _{-0.2}	0.61 ^{+0.18} _{-0.14}	0.72 ^{+0.06} _{-0.07}	52 ⁺² ₋₂	44 ⁺³ ₋₂	189 ⁺³² ₋₂₇	-179010 ⁺²⁶⁰⁶ ₋₂₄₄₅	B	
ESO 452-11	2.1	-26 ⁺¹³ ₋₆	-14 ⁺⁶ ₋₉	112 ⁺³ ₋₈	2.9 ^{+0.1} _{-0.2}	0.06 ^{+0.01} _{-0.03}	0.96 ^{+0.02} _{-0.00}	101 ⁺⁵ ₋₆	26 ⁺² ₋₁	-17 ⁺⁷ ₋₁₁	-202137 ⁺²⁸⁰² ₋₂₃₅₂	B	
NGC 6205	8.6	21 ⁺³ ₋₆	-26 ⁺⁴ ₋₃	87 ⁺³ ₋₃	8.6 ^{+0.2} _{-0.2}	1.01 ^{+0.11} _{-0.07}	0.79 ^{+0.01} _{-0.02}	105 ⁺³ ₋₂	100 ⁺⁴ ₋₁	-185 ⁺²⁹ ₋₁₀	-134382 ⁺¹³⁷⁷ ₋₁₀₀₆	GE	
NGC 6229	29.9	30 ⁺⁶ ₋₈	10 ⁺² ₋₃	58 ⁺⁷ ₋₇	31.0 ^{+1.0} _{-0.8}	0.64 ^{+0.29} _{-0.20}	0.96 ^{+0.01} _{-0.02}	66 ⁺⁸ ₋₆	374 ⁺¹⁴ ₋₁₀	231 ⁺⁴⁹ ₋₇₃	-74500 ⁺¹²⁶³ ₋₁₀₉₁	GE	*
NGC 6218	4.8	-9 ⁺⁴ ₋₄	134 ⁺³ ₋₆	157 ⁺⁴ ₋₅	5.0 ^{+0.2} _{-0.2}	2.25 ^{+0.16} _{-0.13}	0.38 ^{+0.03} _{-0.02}	37 ⁺¹ ₋₁	64 ⁺⁴ ₋₁	578 ⁺³⁰ ₋₃₈	-158304 ⁺¹⁶⁵² ₋₂₃₀₃	D	
FSR 1735	4.3	-80 ⁺¹⁰ ₋₁₂	20 ⁺¹³ ₋₈	174 ⁺¹⁰ ₋₅	4.8 ^{+0.4} _{-0.2}	0.43 ^{+0.19} _{-0.19}	0.84 ^{+0.07} _{-0.07}	82 ⁺³ ₋₃	58 ⁺³ ₋₅	83 ⁺⁵³ ₋₃₅	-167696 ⁺³⁸⁹⁸ ₋₄₂₀₀	LE	*
NGC 6235	4.0	159 ⁺⁴ ₋₃	194 ⁺¹⁷ ₋₂₁	254 ⁺¹⁵ ₋₁₆	6.1 ^{+0.7} _{-0.8}	2.70 ^{+0.32} _{-0.40}	0.39 ^{+0.02} _{-0.02}	53 ⁺⁶ ₋₄	82 ⁺¹¹ ₋₁₀	561 ⁺¹¹⁰ ₋₁₄₁	-145991 ⁺⁵⁸¹⁹ ₋₇₁₉₃	D	
NGC 6254	4.8	-88 ⁺³ ₋₃	134 ⁺⁶ ₋₈	167 ⁺⁴ ₋₅	5.2 ^{+0.2} _{-0.2}	2.13 ^{+0.13} _{-0.16}	0.42 ^{+0.03} _{-0.03}	36 ⁺² ₋₁	78 ⁺¹ ₋₃	604 ⁺²⁶ ₋₄₁	-157521 ⁺¹⁴⁰³ ₋₂₀₀₉	D	
NGC 6256	2.9	-166 ⁺⁹ ₋₈	34 ⁺²³ ₋₂₄	194 ⁺⁶ ₋₄	4.2 ^{+0.6} _{-0.4}	0.19 ^{+0.14} _{-0.13}	0.91 ^{+0.07} _{-0.07}	76 ⁺¹⁰ ₋₉	44 ⁺⁵ ₋₂	94 ⁺⁵⁶ ₋₆₄	-182703 ⁺⁶³²⁴ ₋₃₄₀₁	LE	
Pal 15	38.2	155 ⁺⁸ ₋₉	4 ⁺¹² ₋₇	162 ⁺⁸ ₋₇	54.5 ^{+4.5} _{-2.9}	1.32 ^{+1.37} _{-0.21}	0.95 ^{+0.01} _{-0.04}	85 ⁺¹⁵ ₋₁₈	726 ⁺⁷² ₋₄₅	119 ⁺⁴¹⁴ ₋₃₂₉	-53297 ⁺²⁵⁶⁹ ₋₁₇₃₃	GE	*
NGC 6266	2.0	41 ⁺⁹ ₋₁₄	123 ⁺⁹ ₋₉	146 ⁺⁶ ₋₆	2.5 ^{+0.2} _{-0.4}	0.60 ^{+0.12} _{-0.11}	0.61 ^{+0.03} _{-0.06}	32 ⁺⁴ ₋₂	34 ⁺³ ₋₅	217 ⁺²⁸ ₋₃₇	-205550 ⁺⁴⁸⁷⁹ ₋₆₅₀₀	B	
NGC 6273	1.6	-98 ⁺⁸⁸ ₋₉₇	-239 ⁺¹⁰⁸ ₋₄₁	315 ⁺⁵ ₋₅	3.8 ^{+0.5} _{-0.2}	1.00 ^{+0.21} _{-0.08}	0.59 ^{+0.02} _{-0.04}	109 ⁺¹¹ ₋₁₀	48 ⁺⁶ ₋₂	-144 ⁺⁷⁷ ₋₉₆	-173042 ⁺⁵³¹⁴ ₋₂₅₂₃	LE	
NGC 6284	7.3	14 ⁺² ₋₂	-3 ⁺¹³ ₋₁₄	113 ⁺⁶ ₋₆	7.5 ^{+0.7} _{-0.6}	0.72 ^{+0.16} _{-0.23}	0.82 ^{+0.05} _{-0.02}	91 ⁺⁸ ₋₇	90 ⁺⁸ ₋₆	-19 ⁺⁹³ ₋₉₄	-142286 ⁺⁵¹⁹⁹ ₋₅₀₁₂	GE	
NGC 6287	2.0	-302 ⁺⁹⁶ ₋₇₂	-64 ⁺¹³ ₋₁₈	319 ⁺³ ₋₃	5.3 ^{+0.5} _{-0.3}	0.76 ^{+0.10} _{-0.06}	0.75 ^{+0.02} _{-0.03}	95 ⁺² ₋₂	64 ⁺⁷ ₋₃	-59 ⁺²⁶ ₋₂₈	-158899 ⁺⁴⁸⁰⁴ ₋₂₈₃₈	LE	
NGC 6293	1.8	-152 ⁺⁷ ₋₁₇	-80 ⁺¹² ₋₁₇	232 ⁺⁹ ₋₄	3.6 ^{+0.5} _{-0.3}	0.17 ^{+0.13} _{-0.04}	0.91 ^{+0.02} _{-0.05}	131 ⁺⁷ ₋₁₁	38 ⁺⁵ ₋₃	-93 ⁺²⁹ ₋₅₆	-191506 ⁺⁷⁴⁷⁹ ₋₃₃₇₉	B	
NGC 6304	2.5	79 ⁺⁵ ₋₆	190 ⁺⁵ ₋₃	218 ⁺⁴ ₋₆	3.3 ^{+0.3} _{-0.3}	1.79 ^{+0.20} _{-0.22}	0.29 ^{+0.02} _{-0.01}	20 ⁺¹ ₋₁	52 ⁺⁴ ₋₄	472 ⁺⁵⁶ ₋₅₅	-183230 ⁺⁵⁴⁴⁸ ₋₅₇₉₆	D	
NGC 6316	2.4	102 ⁺⁵ ₋₄	51 ⁺¹³ ₋₁₈	144 ⁺⁸ ₋₇	3.0 ^{+0.4} _{-0.4}	0.40 ^{+0.14} _{-0.23}	0.76 ^{+0.13} _{-0.14}	41 ⁺⁸ ₋₄	36 ⁺⁵ ₋₆	106 ⁺⁴⁵ ₋₅₀	-197198 ⁺⁷⁴⁰⁴ ₋₉₁₅₃	B	
NGC 6341	9.8	50 ⁺⁴ ₋₄	14 ⁺⁴ ₋₅	108 ⁺⁸ ₋₇	10.6 ^{+0.2} _{-0.3}	0.44 ^{+0.16} _{-0.09}	0.92 ^{+0.02} _{-0.03}	78 ⁺⁴ ₋₄	124 ⁺³ ₋₄	121 ⁺³⁵ ₋₃₉	-125452 ⁺¹³⁸³ ₋₁₆₃₃	GE	
NGC 6325	1.3	-80 ⁺³¹ ₋₅₀	-178 ⁺¹³¹ ₋₅₉	209 ⁺²³ ₋₂₃	1.3 ^{+0.5} _{-0.1}	1.06 ^{+0.13} _{-0.31}	0.11 ^{+0.22} _{-0.00}	114 ⁺¹⁴ ₋₁₇	18 ⁺¹¹ ₋₃	-105 ⁺⁷⁸ ₋₈₆	-213001 ⁺⁹⁸⁴³ ₋₄₈₉₀	B	
NGC 6333	1.8	-88 ⁺¹⁴⁶ ₋₉₅	347 ⁺⁸ ₋₄₂	364 ⁺³ ₋₄	6.5 ^{+0.5} _{-0.3}	0.97 ^{+0.16} _{-0.14}	0.74 ^{+0.03} _{-0.03}	59 ⁺⁴ ₋₄	74 ⁺⁶ ₋₂	327 ⁺⁵⁶ ₋₅₆	-151332 ⁺³⁸⁸¹ ₋₂₉₁₁	LE	
NGC 6342	1.6	-25 ⁺⁷⁵ ₋₆₅	164 ⁺⁸ ₋₄₂	169 ⁺⁴ ₋₃	1.7 ^{+0.2} _{-0.1}	0.89 ^{+0.14} _{-0.17}	0.31 ^{+0.13} _{-0.08}	64 ⁺³ ₋₃	24 ⁺⁷ ₋₂	117 ⁺¹⁹ ₋₁₇	-206944 ⁺³⁹⁵⁰ ₋₁₃₀₄	B	
NGC 6356	7.2	48 ⁺⁶ ₋₅	105 ⁺¹⁶ ₋₁₉	156 ⁺¹¹ ₋₉	7.9 ^{+0.7} _{-0.5}	2.37 ^{+0.57} _{-0.53}	0.54 ^{+0.08} _{-0.07}	42 ⁺⁵ ₋₃	102 ⁺¹¹ ₋₆	701 ⁺¹³⁶ ₋₁₄₀	-136904 ⁺⁵²³² ₋₄₁₅₅	D	
NGC 6355	1.2	-207 ⁺⁷ ₋₉	-106 ⁺⁵¹ ₋₂₈	274 ⁺⁶ ₋₆	2.2 ^{+0.8} _{-0.5}	0.64 ^{+0.09} _{-0.11}	0.55 ^{+0.12} _{-0.09}	106 ⁺⁶ ₋₇	28 ⁺¹⁰ ₋₅	-91 ⁺⁴⁸ ₋₅₆	-199376 ⁺¹¹²⁸⁸ ₋₉₉₂₉	B	
NGC 6352	3.6	43 ⁺¹¹ ₋₁₀	226 ⁺⁵ ₋₇	230 ⁺⁴ ₋₅	4.1 ^{+0.3} _{-0.3}	3.17 ^{+0.14} _{-0.16}	0.13 ^{+0.03} _{-0.03}	12 ⁺¹ ₋₁	68 ⁺⁴ ₋₅	792 ⁺⁵⁰ ₋₄₈	-163943 ⁺³³³² ₋₃₁₇₄	D	
IC 1257	17.6	-48 ⁺⁶ ₋₆	-37 ⁺⁹ ₋₁₀	63 ⁺⁶ ₋₃	18.1 ^{+1.0} _{-0.8}	1.24 ^{+0.45} _{-0.32}	0.87 ^{+0.03} _{-0.04}	158 ⁺² ₋₄	206 ⁺¹¹ ₋₁₀	-600 ⁺¹⁴¹ ₋₁₆₂	-99053 ⁺²⁴⁵⁸ ₋₂₂₉₂	GE	

Name	d_{GC} [kpc]	II [km/s]	Θ [km/s]	V_{tot} [km/s]	apo [kpc]	peri [kpc]	ecc	incl. θ [deg]	T_r [Gyr]	L_Z [kpc km/s]	E [km ² /s ²]	Galactic Sub- system
Terzan 2	1.0	-120 ⁺³⁰ ₋₁₇	-47 ⁺²² ₋₃₂	137 ⁺³ ₋₂	1.2 ^{+0.4} _{-0.3}	0.09 ^{+0.04} _{-0.02}	0.86 ^{+0.07} _{-0.13}	160 ⁺⁴ ₋₁₈	14 ⁺⁵ ₋₄	-44 ⁺¹³ ₋₁₃	-242209 ⁺¹³⁷⁸² ₋₁₄₃₆₅	B
NGC 6366	5.3	94 ⁺³ ₋₂	134 ⁺³ ₋₄	175 ⁺³ ₋₃	5.8 ^{+0.2} _{-0.2}	2.20 ^{+0.09} _{-0.11}	0.45 ^{+0.02} _{-0.01}	32 ⁺¹ ₋₁	74 ⁺³ ₋₁	697 ⁺²⁸ ₋₃₁	-153394 ⁺¹⁵⁹⁹ ₋₁₆₆₃	D
Terzan 4	1.2	20 ⁺⁹ ₋₁₆	67 ⁺¹¹ ₋₉	118 ⁺⁷ ₋₆	1.3 ^{+0.4} _{-0.3}	0.20 ^{+0.06} _{-0.03}	0.73 ^{+0.04} _{-0.09}	54 ⁺⁴ ₋₄	14 ⁺⁴ ₋₄	82 ⁺²³ ₋₂₁	-235193 ⁺¹¹⁹⁷⁴ ₋₁₅₄₄₉	B
BH 229	0.5	5 ⁺³¹ ₋₃₂	-54 ⁺²⁵ ₋₅	293 ⁺¹² ₋₁₄	0.8 ^{+0.7} _{-0.1}	0.28 ^{+0.12} _{-0.10}	0.49 ^{+0.23} _{-0.09}	100 ⁺¹ ₋₅	10 ⁺⁶ ₋₁	10 ⁺⁶ ₋₁₀	-249619 ⁺²²⁸⁰⁵ ₋₁₇₁₄	B
FSR 1758	3.7	63 ⁺²⁶ ₋₂₇	-341 ⁺⁶ ₋₄	401 ⁺⁶ ₋₅	13.8 ^{+1.9} _{-1.4}	3.66 ^{+0.40} _{-0.33}	0.58 ^{+0.02} _{-0.01}	147 ⁺¹ ₋₁	174 ⁺²⁴ ₋₁₈	-1254 ⁺¹¹⁶ ₋₁₃₁	-108059 ⁺⁶²⁵⁰ ₋₅₄₈₅	Seq
NGC 6362	5.2	18 ⁺¹⁴ ₋₇	124 ⁺⁹ ₋₇	160 ⁺⁷ ₋₅	5.3 ^{+0.2} _{-0.1}	2.46 ^{+0.23} _{-0.17}	0.37 ^{+0.03} _{-0.03}	45 ⁺³ ₋₃	70 ⁺⁵ ₋₁	583 ⁺³⁵ ₋₁₆₃₂	-153483 ⁺²⁷⁰³ ₋₁₆₃₂	D
Liller 1	0.8	97 ⁺²⁰ ₋₂₆	-55 ⁺⁷² ₋₁₇	115 ⁺¹¹ ₋₁₆	0.8 ^{+0.2} _{-0.0}	0.09 ^{+0.06} _{-0.07}	0.81 ^{+0.14} _{-0.07}	155 ⁺⁸ ₋₈₉	8 ⁺⁴ ₋₀	-41 ⁺²³ ₋₂₃	-262426 ⁺¹²¹⁷⁴ ₋₂₅₁₄	B
NGC 6380	3.1	-59 ⁺⁷ ₋₈	-29 ⁺¹¹ ₋₁₀	67 ⁺¹⁰ ₋₈	3.4 ^{+0.4} _{-0.4}	0.16 ^{+0.21} _{-0.03}	0.91 ^{+0.01} _{-0.09}	168 ⁺⁴ ₋₈	38 ⁺⁶ ₋₃	-89 ⁺³⁹ ₋₄₇	-195003 ⁺⁷¹⁵⁷ ₋₅₅₆₂	B
Terzan 1	1.6	-74 ⁺² ₋₄	65 ⁺⁹ ₋₁₀	99 ⁺⁸ ₋₆	1.8 ^{+0.3} _{-0.3}	0.21 ^{+0.07} _{-0.05}	0.78 ^{+0.03} _{-0.04}	5 ⁺³ ₋₁	22 ⁺⁴ ₋₅	106 ⁺²⁶ ₋₂₈	-224589 ⁺⁶⁹⁴² ₋₉₇₀₀	B
Pismis 26	1.4	-105 ⁺⁶³ ₋₄₆	204 ⁺²⁵ ₋₇	302 ⁺⁷ ₋₇	3.0 ^{+0.5} _{-0.2}	0.92 ^{+0.43} _{-0.28}	0.54 ^{+0.14} _{-0.16}	41 ⁺⁴ ₋₂	42 ⁺¹¹ ₋₂	271 ⁺⁶² ₋₅₀	-188443 ⁺⁵⁶⁶⁷ ₋₂₀₆₀	LE
NGC 6388	3.0	-65 ⁺¹² ₋₁₇	-93 ⁺¹⁴ ₋₁₀	115 ⁺⁷ ₋₅	3.5 ^{+0.2} _{-0.3}	0.62 ^{+0.22} _{-0.11}	0.70 ^{+0.03} _{-0.08}	148 ⁺⁵ ₋₇	44 ⁺² ₋₂	-255 ⁺⁴⁹ ₋₄₅	-190244 ⁺³⁵⁵⁰ ₋₂₇₀₂	Seq
NGC 6402	4.0	-20 ⁺¹⁵ ₋₁₆	49 ⁺⁵ ₋₇	56 ⁺⁸ ₋₅	4.8 ^{+0.1} _{-0.4}	0.29 ^{+0.12} _{-0.02}	0.88 ^{+0.04} _{-0.04}	46 ⁺⁷ ₋₅	52 ⁺³ ₋₃	159 ⁺¹⁹ ₋₂₅	-176490 ⁺²⁶⁵⁴ ₋₁₉₃₇	LE
NGC 6401	2.5	-30 ⁺²² ₋₁₆	-255 ⁺³ ₋₃	301 ⁺⁵ ₋₄	4.5 ^{+0.6} _{-0.6}	2.37 ^{+0.46} _{-0.45}	0.31 ^{+0.04} _{-0.03}	144 ⁺¹ ₋₁	62 ⁺¹² ₋₉	-598 ⁺¹¹⁶ ₋₁₁₆	-162266 ⁺⁸⁰⁰⁴ ₋₈₅₈₆	Seq
NGC 6397	6.3	36 ⁺⁴ ₋₅	127 ⁺⁷ ₋₇	178 ⁺⁶ ₋₆	6.5 ^{+0.1} _{-0.1}	2.76 ^{+0.20} _{-0.20}	0.41 ^{+0.03} _{-0.03}	43 ⁺² ₋₂	84 ⁺⁴ ₋₁	793 ⁺⁴¹ ₋₄₂	-144589 ⁺¹³⁵⁰ ₋₁₅₁₆	D
Pal 6	2.5	-191 ⁺¹ ₋₃	22 ⁺⁸ ₋₁₁	245 ⁺⁴ ₋₄	4.5 ^{+0.4} _{-0.6}	0.19 ^{+0.02} _{-0.06}	0.95 ^{+0.02} _{-0.02}	83 ⁺⁴ ₋₃	44 ⁺⁴ ₋₄	55 ⁺²⁰ ₋₂₉	-179517 ⁺⁴²⁸³ ₋₇₀₇₈	LE
NGC 6426	14.3	-111 ⁺¹³ ₋₁₂	92 ⁺¹³ ₋₁₃	147 ⁺¹⁴ ₋₁₄	16.6 ^{+0.9} _{-0.8}	3.17 ^{+0.67} _{-0.55}	0.68 ^{+0.04} _{-0.05}	26 ⁺³ ₋₃	200 ⁺¹⁷ ₋₁₂	1204 ⁺²⁰⁴ ₋₁₉₃	-100803 ⁺³²⁷² ₋₂₉₇₅	H99
Djorg 1	1.2	-255 ⁺¹⁶¹ ₋₆₅	311 ⁺⁵⁹ ₋₃₄	402 ⁺⁹ ₋₇	5.9 ^{+1.4} _{-1.7}	0.77 ^{+0.15} _{-0.07}	0.77 ^{+0.01} _{-0.07}	24 ⁺⁷ ₋₄	66 ⁺¹⁵ ₋₁₆	346 ⁺⁶⁷ ₋₈₀	-162360 ⁺¹¹⁹⁵¹ ₋₁₇₅₀₈	GE
Terzan 5	1.5	76 ⁺⁵ ₋₅	50 ⁺³ ₋₁₁	96 ⁺⁷ ₋₇	1.7 ^{+0.4} _{-0.3}	0.14 ^{+0.03} _{-0.07}	0.84 ^{+0.04} _{-0.04}	40 ⁺⁶ ₋₆	18 ⁺⁴ ₋₄	75 ⁺²⁶ ₋₂₆	-228141 ⁺⁹⁹⁰⁹ ₋₁₉₆₇₇	B
NGC 6440	1.3	82 ⁺¹⁰ ₋₂₁	-41 ⁺³⁰ ₋₂₉	100 ⁺⁸ ₋₇	1.4 ^{+0.3} _{-0.0}	0.16 ^{+0.07} _{-0.09}	0.80 ^{+0.10} _{-0.06}	116 ⁺¹⁸ ₋₂₀	14 ⁺⁴ ₋₀	-46 ⁺³⁸ ₋₄₄	-232585 ⁺⁶⁸⁹⁸ ₋₈₅₇	B
NGC 6441	3.6	16 ⁺⁹ ₋₈	67 ⁺¹⁴ ₋₁₅	72 ⁺¹⁵ ₋₁₄	3.6 ^{+0.6} _{-0.4}	0.75 ^{+0.21} _{-0.21}	0.66 ^{+0.07} _{-0.06}	22 ⁺⁵ ₋₃	42 ⁺⁷ ₋₄	230 ⁺⁶⁹ ₋₆₃	-186246 ⁺⁷⁸⁴¹ ₋₆₉₉₃	LE
Terzan 6	1.5	-137 ⁺³ ₋₃	-51 ⁺¹⁴ ₋₁₄	147 ⁺⁵ ₋₃	1.9 ^{+0.4} _{-0.4}	0.15 ^{+0.07} _{-0.04}	0.85 ^{+0.03} _{-0.05}	170 ⁺³ ₋₇	22 ⁺⁷ ₋₄	-77 ⁺²⁶ ₋₂₈	-221047 ⁺¹⁰⁰⁹⁸ ₋₁₁₄₈₆	B
NGC 6453	3.4	-105 ⁺⁶ ₋₅	39 ⁺¹³ ₋₁₃	197 ⁺⁸ ₋₈	3.9 ^{+0.5} _{-0.7}	0.99 ^{+0.19} _{-0.14}	0.59 ^{+0.05} _{-0.07}	78 ⁺⁴ ₋₄	54 ⁺⁶ ₋₈	132 ⁺³⁷ ₋₅₁	-172359 ⁺⁶⁴⁴⁶ ₋₉₀₁₇	LE
NGC 6496	4.0	-35 ⁺³² ₋₃₄	322 ⁺¹⁶ ₋₂₆	330 ⁺¹⁶ ₋₂₂	9.2 ^{+1.5} _{-1.4}	3.73 ^{+0.38} _{-0.35}	0.42 ^{+0.05} _{-0.06}	32 ⁺² ₋₂	120 ⁺¹⁸ ₋₁₆	1118 ⁺¹²⁹ ₋₁₄₄	-125956 ⁺⁷⁰⁷⁶ ₋₇₉₄₈	D
Terzan 9	1.3	-53 ⁺⁹ ₋₆	15 ⁺¹⁵ ₋₉	82 ⁺³ ₋₃	1.4 ^{+0.3} _{-0.4}	0.05 ^{+0.04} _{-0.02}	0.93 ^{+0.03} _{-0.08}	78 ⁺⁷ ₋₁₁	16 ⁺³ ₋₅	19 ⁺¹¹ ₋₁₁	-235578 ⁺⁹¹⁵⁰ ₋₁₆₄₁₉	B
Djorg 2	2.0	162 ⁺⁵ ₋₃	159 ⁺³ ₋₆	232 ⁺² ₋₃	3.2 ^{+0.3} _{-0.4}	0.91 ^{+0.14} _{-0.18}	0.56 ^{+0.03} _{-0.02}	12 ⁺¹ ₋₁	42 ⁺⁵ ₋₄	323 ⁺⁴³ ₋₅₈	-191864 ⁺⁴⁸⁶⁴ ₋₇₂₁₄	B
NGC 6517	4.0	47 ⁺⁸ ₋₁₃	42 ⁺⁹ ₋₆	73 ⁺⁵ ₋₄	4.5 ^{+0.1} _{-0.3}	0.31 ^{+0.14} _{-0.04}	0.87 ^{+0.02} _{-0.06}	52 ⁺⁵ ₋₇	50 ⁺³ ₋₂	161 ⁺³² ₋₂₅	-179254 ⁺²⁴⁷⁸ ₋₃₀₁₈	LE
Terzan 10	2.2	229 ⁺⁸ ₋₁₃	92 ⁺²⁷ ₋₁₇	338 ⁺⁸ ₋₉	5.8 ^{+0.8} _{-1.0}	0.68 ^{+0.14} _{-0.12}	0.79 ^{+0.02} _{-0.04}	71 ⁺³ ₋₅	74 ⁺¹⁰ ₋₁₁	204 ⁺²⁴ ₋₂₅	-157214 ⁺⁷⁷⁰² ₋₁₀₆₈₅	GE
NGC 6522	0.8	34 ⁺²¹ ₋₁₃	91 ⁺²⁵ ₋₁₇	211 ⁺¹³ ₋₉	1.2 ^{+0.4} _{-0.2}	0.23 ^{+0.18} _{-0.13}	0.67 ^{+0.13} _{-0.10}	63 ⁺¹² ₋₇	16 ⁺⁹ ₋₅	58 ⁺⁴¹ ₋₂₇	-238928 ⁺¹⁹²⁶⁶ ₋₁₁₆₃₉	B
NGC 6535	4.0	92 ⁺⁷ ₋₇	-83 ⁺⁵ ₋₇	131 ⁺³ ₋₃	4.6 ^{+0.2} _{-0.2}	1.00 ^{+0.09} _{-0.09}	0.64 ^{+0.04} _{-0.02}	160 ⁺¹ ₋₁	56 ⁺² ₋₂	-320 ⁺²⁶ ₋₂₈	-173165 ⁺²⁵⁴³ ₋₁₉₈₈	Seq
NGC 6528	0.7	-196 ⁺¹⁷ ₋₅₈	111 ⁺⁶⁴ ₋₃₁	229 ⁺² ₋₂	1.1 ^{+0.5} _{-0.5}	0.25 ^{+0.18} _{-0.06}	0.61 ^{+0.14} _{-0.39}	71 ⁺⁴ ₋₃	14 ⁺⁵ ₋₄	50 ⁺¹² ₋₁₅	-241754 ⁺¹²⁹⁵⁰ ₋₁₂₂₈₄	B
NGC 6539	3.1	-2 ⁺¹⁵ ₋₁₈	118 ⁺⁵ ₋₇	208 ⁺⁹ ₋₆	3.4 ^{+0.2} _{-0.1}	1.86 ^{+0.23} _{-0.19}	0.29 ^{+0.04} _{-0.04}	56 ⁺² ₋₂	56 ⁺⁶ ₋₈	347 ⁺²⁶ ₋₂₈	-174408 ⁺³⁵⁸⁵ ₋₂₆₈₀	D
NGC 6540	3.0	13 ⁺² ₋₂	148 ⁺⁵ ₋₆	159 ⁺⁵ ₋₆	3.1 ^{+0.2} _{-0.3}	1.60 ^{+0.12} _{-0.18}	0.32 ^{+0.03} _{-0.03}	21 ⁺¹ ₋₁	48 ⁺² ₋₄	450 ⁺³³ ₋₄₉	-187451 ⁺³³⁰⁶ ₋₅₁₂₅	D
NGC 6544	5.3	6 ⁺² ₋₂	6 ⁺¹² ₋₇	91 ⁺⁶ ₋₄	5.7 ^{+0.1} _{-0.3}	0.06 ^{+0.15} _{-0.03}	0.98 ^{+0.01} _{-0.05}	86 ⁺⁴ ₋₈	52 ⁺⁴ ₋₁	30 ⁺⁶⁷ ₋₃₇	-166552 ⁺¹⁵⁰⁰ ₋₁₈₆₁	GE
NGC 6541	2.3	124 ⁺²³ ₋₄₃	192 ⁺²² ₋₁₆	253 ⁺⁶ ₋₄	3.8 ^{+0.4} _{-0.4}	1.25 ^{+0.17} _{-0.10}	0.50 ^{+0.06} _{-0.08}	40 ⁺⁴ ₋₃	50 ⁺⁴ ₋₄	333 ⁺²² ₋₂₀	-175234 ⁺³³⁸³ ₋₃₄₀₉	LE
ESO 280-06	13.8	34 ⁺⁷ ₋₆	27 ⁺¹⁶ ₋₁₃	86 ⁺¹⁰ ₋₆	14.2 ^{+0.9} _{-0.9}	1.00 ^{+0.56} _{-0.39}	0.87 ^{+0.04} _{-0.06}	67 ⁺¹¹ ₋₁₂	164 ⁺¹² ₋₁₅	346 ⁺²¹⁶ ₋₁₇₈	-110196 ⁺³⁴⁶⁵ ₋₃₂₉₈	GE
NGC 6553	2.4	46 ⁺⁸ ₋₆	246 ⁺¹ ₋₂	250 ⁺¹ ₋₁	3.3 ^{+0.2} _{-0.3}	2.27 ^{+0.39} _{-0.33}	0.19 ^{+0.03} _{-0.02}	7 ⁺¹ ₋₁	52 ⁺³ ₋₃	589 ⁺⁶⁷ ₋₈₀	-179761 ⁺⁴⁷⁰⁶ ₋₆₂₁₈	D
NGC 6558	1.2	187 ⁺² ₋₁	93 ⁺⁹ ₋₉	210 ⁺⁵ ₋₄	1.7 ^{+0.6} _{-0.4}	0.28 ^{+0.12} _{-0.06}	0.72 ^{+0.10} _{-0.14}	63 ⁺⁸ ₋₉	20 ⁺⁶ ₋₄	88 ⁺³⁹ ₋₃₀	-217022 ⁺¹⁰⁴⁹² ₋₉₄₁₆	B
Pal 7	3.9	-77 ⁺¹⁵ ₋₉	267 ⁺⁷ ₋₆	279 ⁺⁵ ₋₅	6.0 ^{+0.3} _{-0.4}	3.52 ^{+0.11} _{-0.17}	0.26 ^{+0.02} _{-0.02}	11 ⁺¹ ₋₀	86 ⁺⁴ ₋₄	1034 ⁺⁴⁰ ₋₅₉	-147446 ⁺²³⁴⁸ ₋₃₄₇₀	D

*

Name	d_{GC} [kpc]	II [km/s]	Θ [km/s]	V_{tot} [km/s]	apo [kpc]	peri [kpc]	ecc	incl. θ [deg]	T_r [Gyr]	Lz [kpc km/s]	E [km ² /s ²]	Gal. Sub- syst	
Terzan 12	3.6	-97 ⁺³ ₋₃	165 ⁺⁶ ₋₇	213 ⁺⁴ ₋₅	4.4 ^{+0.3} _{-0.3}	2.09 ^{+0.11} _{-0.14}	0.35 ^{+0.03} _{-0.01}	29 ⁺¹ ₋₂	60 ⁺⁴ ₋₂	599 ⁺⁴⁰ ₋₃₈	-169045 ⁺³⁴⁰⁷ ₋₃₂₁₅	D	
NGC 6569	2.8	-40 ⁺² ₋₂	179 ⁺²⁴ ₋₁₉	185 ⁺²³ ₋₁₈	3.0 ^{+0.6} _{-0.4}	1.92 ^{+0.52} _{-0.44}	0.22 ^{+0.09} _{-0.06}	26 ⁺⁶ ₋₅	56 ⁺¹⁰ ₋₈	451 ⁺¹³³ ₋₁₀₁	-181599 ⁺⁹⁷¹⁷ ₋₇₇₁₇	D	*
ESO 456-78	2.0	71 ⁺⁹ ₋₇	198 ⁺³ ₋₅	251 ⁺⁵ ₋₆	2.9 ^{+0.3} _{-0.3}	1.43 ^{+0.31} _{-0.30}	0.34 ^{+0.06} _{-0.05}	34 ⁺¹ ₋₂	52 ⁺⁵ ₋₈	371 ⁺⁶⁹ ₋₆₃	-186882 ⁺⁶⁵⁶⁶ ₋₇₁₈₃	D	
NGC 6584	6.8	198 ⁺¹⁶ ₋₁₇	100 ⁺¹⁹ ₋₂₆	324 ⁺¹³ ₋₁₅	18.0 ^{+2.1} _{-2.1}	1.68 ^{+0.51} _{-0.56}	0.83 ^{+0.05} _{-0.04}	51 ⁺⁶ ₋₄	212 ⁺²⁷ ₋₂₇	565 ⁺¹⁴¹ ₋₁₇₅	-98062 ⁺⁵⁰⁸³ ₋₆₁₆₅	GE	
NGC 6624	1.2	-29 ⁺⁴⁴ ₋₂₀	59 ⁺⁸ ₋₁₅	137 ⁺⁷ ₋₄	1.6 ^{+0.2} _{-0.2}	0.13 ^{+0.14} _{-0.06}	0.85 ^{+0.06} _{-0.12}	73 ⁺² ₋₄	22 ⁺² ₋₅	36 ⁺¹⁷ ₋₁₃	-226289 ⁺⁷⁸¹⁸ ₋₃₈₆₆	B	
NGC 6626	3.0	-27 ⁺³ ₋₃	57 ⁺⁹ ₋₉	113 ⁺⁶ ₋₆	3.1 ^{+0.3} _{-0.2}	0.45 ^{+0.09} _{-0.12}	0.75 ^{+0.05} _{-0.05}	60 ⁺⁴ ₋₄	42 ⁺⁵ ₋₃	169 ⁺³⁰ ₋₂₉	-193005 ⁺⁴⁰⁷³ ₋₃₄₅₉	B	
NGC 6638	2.0	68 ⁺⁴ ₋₈	14 ⁺¹⁰ ₋₁₇	74 ⁺⁶ ₋₆	2.4 ^{+0.4} _{-0.2}	0.05 ^{+0.05} _{-0.02}	0.96 ^{+0.02} _{-0.05}	80 ⁺¹³ ₋₇	20 ⁺⁶ ₋₀	22 ⁺¹³ ₋₀	-212090 ⁺⁷²⁸³ ₋₂₉₁₄	B	
NGC6637	1.6	35 ⁺⁴⁰ ₋₈₃	90 ⁺⁴ ₋₄₂	126 ⁺⁷ ₋₄	2.3 ^{+0.2} _{-0.3}	0.09 ^{+0.17} _{-0.06}	0.93 ^{+0.05} _{-0.15}	77 ⁺⁶ ₋₆	22 ⁺² ₋₁	40 ⁺³⁰ ₋₂₀	-212857 ⁺⁴⁸²² ₋₁₇₇₄	B	
NGC 6642	1.7	112 ⁺⁵ ₋₁₃	25 ⁺²² ₋₃₈	126 ⁺⁵ ₋₈	2.2 ^{+0.2} _{-0.1}	0.08 ^{+0.07} _{-0.04}	0.93 ^{+0.03} _{-0.05}	46 ⁺⁶⁵ ₋₁₉	24 ⁺³ ₋₂	36 ⁺⁴⁰ ₋₅₄	-215381 ⁺³⁷⁰⁹ ₋₁₇₈₃	B	
NGC 6652	2.5	-55 ⁺⁴ ₋₁	30 ⁺¹¹ ₋₁₆	184 ⁺⁷ ₋₆	4.2 ^{+0.3} _{-0.2}	0.08 ^{+0.16} _{-0.07}	0.96 ^{+0.03} _{-0.06}	75 ⁺⁸ ₋₃	38 ⁺⁶ ₋₂	46 ⁺³⁵ ₋₂₈	-183873 ⁺⁶⁶⁸⁵ ₋₂₃₇₄	B	
NGC 6656	5.2	176 ⁺² ₋₁	200 ⁺¹ ₋₁	302 ⁺⁵ ₋₄	9.8 ^{+0.3} _{-0.3}	3.05 ^{+0.11} _{-0.09}	0.53 ^{+0.00} _{-0.01}	33 ⁺² ₋₂	126 ⁺⁴ ₋₅	1041 ⁺³¹ ₋₃₃	-125541 ⁺¹⁹¹⁰ ₋₁₆₉₀	D	
Pal 8	5.3	-22 ⁺¹³ ₋₁₆	118 ⁺¹⁴ ₋₁₃	125 ⁺¹⁵ ₋₁₃	5.6 ^{+0.4} _{-0.6}	1.79 ^{+0.26} _{-0.32}	0.52 ^{+0.04} _{-0.09}	24 ⁺² ₋₂	72 ⁺⁶ ₋₆	601 ⁺¹⁰³ ₋₈₉	-159674 ⁺⁵⁵⁶¹ ₋₄₅₇₈	D	
NGC 6681	2.0	219 ⁺³⁵ ₋₁₂₀	57 ⁺¹¹³ ₋₅₀	287 ⁺⁸ ₋₅	4.5 ^{+0.6} _{-0.4}	0.67 ^{+0.32} _{-0.20}	0.74 ^{+0.09} _{-0.12}	84 ⁺⁹ ₋₇	52 ⁺⁵ ₋₂	37 ⁺⁵¹ ₋₄₁	-168029 ⁺⁴⁶⁶⁹ ₋₂₂₂₇	LE	
NGC 6712	3.6	145 ⁺³ ₋₂	25 ⁺¹³ ₋₁₀	208 ⁺⁴ ₋₆	5.5 ^{+0.2} _{-0.4}	0.18 ^{+0.10} _{-0.08}	0.94 ^{+0.02} _{-0.04}	79 ⁺⁴ ₋₆	58 ⁺² ₋₅	92 ⁺⁵³ ₋₃₈	-168520 ⁺³³⁵⁴ ₋₃₃₃₅	GE	
NGC 6715	18.6	231 ⁺⁵ ₋₄	51 ⁺¹⁴ ₋₁₃	313 ⁺⁹ ₋₇	53.9 ^{+10.6} _{-6.8}	14.66 ^{+1.02} _{-0.92}	0.57 ^{+0.04} _{-0.03}	80 ⁺³ ₋₃	862 ⁺¹⁸⁹ ₋₁₁₈	886 ⁺²⁴⁴ ₋₂₃₃	-49410 ⁺⁴⁹⁰⁰ ₋₃₉₇₆	Sgr	
NGC 6717	2.5	-11 ⁺¹⁴ ₋₁₇	115 ⁺⁵ ₋₉	118 ⁺⁶ ₋₇	3.1 ^{+0.2} _{-0.5}	0.65 ^{+0.21} _{-0.06}	0.65 ^{+0.01} _{-0.10}	32 ⁺³ ₋₄	34 ⁺⁵ ₋₁	249 ⁺³³ ₋₃₂	-195877 ⁺⁴⁴⁵⁶ ₋₃₇₀₃	B	
NGC 6723	2.6	101 ⁺¹² ₋₁₉	-179 ⁺³³⁴ ₋₁₇	209 ⁺⁴ ₋₄	3.1 ^{+0.2} _{-0.2}	1.84 ^{+0.18} _{-0.19}	0.26 ^{+0.03} _{-0.03}	90 ⁺⁸ ₋₇	40 ⁺⁴ ₋₁	-2 ⁺⁶⁶ ₋₇₅	-175214 ⁺³³⁰⁴ ₋₂₄₅₆	B	
NGC 6749	5.0	-23 ⁺¹⁴ ₋₁₄	110 ⁺⁸ ₋₈	112 ⁺⁷ ₋₉	5.1 ^{+0.2} _{-0.2}	1.55 ^{+0.17} _{-0.3}	0.53 ^{+0.04} _{-0.03}	3 ⁺⁰ ₋₀	62 ⁺¹ ₋₁	555 ⁺⁴¹ ₋₄₁	-167074 ⁺³⁰⁶² ₋₂₂₄₇	D	
NGC 6752	5.5	-24 ⁺³ ₋₃	179 ⁺⁵ ₋₃	190 ⁺⁵ ₋₃	5.7 ^{+0.2} _{-0.2}	3.57 ^{+0.21} _{-0.15}	0.23 ^{+0.01} _{-0.02}	24 ⁺¹ ₋₁	82 ⁺⁴ ₋₂	932 ⁺⁴⁷ ₋₃₈	-147118 ⁺¹⁹⁹⁷ ₋₁₈₄₁	D	
NGC 6760	5.0	91 ⁺¹⁰ ₋₁₀	147 ⁺⁶ ₋₆	173 ⁺⁵ ₋₅	5.6 ^{+0.2} _{-0.2}	2.17 ^{+0.19} _{-0.18}	0.44 ^{+0.03} _{-0.03}	6 ⁺⁰ ₋₀	72 ⁺³ ₋₃	725 ⁺⁵² ₋₅₀	-158822 ⁺²⁶²⁶ ₋₂₄₀₁	D	
NGC 6779	9.3	154 ⁺¹ ₋₁	-14 ⁺⁶ ₋₄	184 ⁺³ ₋₃	12.5 ^{+0.5} _{-0.7}	0.25 ^{+0.15} _{-0.06}	0.96 ^{+0.01} _{-0.02}	100 ⁺³ ₋₄	134 ⁺⁶ ₋₈	-129 ⁺⁵⁷ ₋₄₀	-119887 ⁺²⁶¹⁴ ₋₃₀₀₉	GE	
Terzan 7	15.3	259 ⁺⁶ ₋₆	32 ⁺¹⁴ ₋₁₅	319 ⁺⁹ ₋₈	42.3 ^{+6.5} _{-4.7}	12.73 ^{+0.75} _{-0.68}	0.54 ^{+0.03} _{-0.03}	85 ⁺³ ₋₂	656 ⁺¹⁰⁹ ₋₇₅	422 ⁺¹⁸⁰ ₋₂₀₀	-56985 ⁺⁴³⁸¹ ₋₃₇₆₀	Sgr	
Pal 10	6.6	-64 ⁺¹⁰ ₋₁₀	187 ⁺⁸ ₋₈	198 ⁺⁸ ₋₈	7.2 ^{+0.3} _{-0.2}	4.00 ^{+0.29} _{-0.25}	0.28 ^{+0.03} _{-0.02}	7 ⁺⁰ ₋₀	100 ⁺⁵ ₋₃	1240 ⁺⁶⁹ ₋₆₉	-137907 ⁺²⁵⁹¹ ₋₂₀₅₀	D	
Arp 2	21.2	242 ⁺⁶ ₋₈	61 ⁺¹⁸ ₋₁₁	306 ⁺⁸ ₋₇	61.3 ^{+9.4} _{-7.0}	17.54 ^{+0.89} _{-0.77}	0.55 ^{+0.04} _{-0.04}	79 ⁺² ₋₃	1026 ⁺¹⁶⁹ ₋₁₂₅	1128 ⁺³²⁷ ₋₂₁₃	-45162 ⁺³⁴⁸³ ₋₃₀₈₁	Sgr	
NGC 6809	4.1	-199 ⁺³ ₋₄	75 ⁺¹¹ ₋₁₃	220 ⁺³ ₋₂	5.7 ^{+0.3} _{-0.3}	1.18 ^{+0.15} _{-0.14}	0.66 ^{+0.04} _{-0.04}	68 ⁺⁴ ₋₃	76 ⁺³ ₋₃	262 ⁺⁴¹ ₋₄₆	-154418 ⁺²⁷²¹ ₋₂₂₉₄	LE	
Terzan 8	19.1	269 ⁺⁷ ₋₆	41 ⁺¹² ₋₁₇	317 ⁺⁹ ₋₇	60.0 ^{+9.7} _{-6.9}	16.12 ^{+0.88} _{-0.76}	0.58 ^{+0.03} _{-0.04}	83 ⁺³ ₋₂	982 ⁺¹⁷⁴ ₋₁₂₁	646 ⁺¹⁷¹ ₋₂₆₇	-46155 ⁺³⁷²⁶ ₋₃₁₇₇	Sgr	
Pal 11	8.1	-17 ⁺¹⁵ ₋₁₉	138 ⁺⁹ ₋₁₂	140 ⁺¹¹ ₋₁₂	8.2 ^{+0.4} _{-0.3}	3.47 ^{+0.37} _{-0.45}	0.40 ^{+0.06} _{-0.04}	27 ⁺² ₋₂	110 ⁺⁷ ₋₅	1012 ⁺⁸¹ ₋₁₀₇	-132025 ⁺²⁵⁵⁵ ₋₂₇₀₄	D	
NGC 6838	7.0	38 ⁺⁵ ₋₅	204 ⁺³ ₋₂	211 ⁺² ₋₂	7.3 ^{+0.2} _{-0.1}	5.00 ^{+0.13} _{-0.11}	0.18 ^{+0.02} _{-0.01}	12 ⁺⁰ ₋₀	110 ⁺³ ₋₁	1422 ⁺²⁸ ₋₂₅	-132364 ⁺¹⁷⁰⁷ ₋₉₄₁	D	
NGC 6864	14.6	-98 ⁺⁸ ₋₇	21 ⁺¹¹ ₋₁₃	112 ⁺⁸ ₋₈	16.5 ^{+0.8} _{-0.7}	0.59 ^{+0.47} _{-0.23}	0.93 ^{+0.03} _{-0.03}	56 ⁺²⁰ ₋₁₉	186 ⁺¹⁰ ₋₁₇	238 ⁺¹³⁶ ₋₁₄₇	-103497 ⁺²⁴⁴⁰ ₋₂₂₂₃	GE	
NGC 6934	12.7	-290 ⁺¹⁴ ₋₁₃	105 ⁺²⁰ ₋₂₂	332 ⁺¹² ₋₁₂	41.4 ^{+5.4} _{-5.2}	2.57 ^{+0.74} _{-0.50}	0.88 ^{+0.02} _{-0.03}	23 ⁺³ ₋₁	528 ⁺⁸³ ₋₇₆	1224 ⁺²²⁸ ₋₂₆₇	-62807 ⁺⁴³⁰¹ ₋₄₉₈₄	GE	
NGC 6981	12.8	-158 ⁺¹¹ ₋₉	2 ⁺¹⁵ ₋₁₁	232 ⁺⁷ ₋₇	22.5 ^{+1.2} _{-0.8}	0.38 ^{+0.10} _{-0.23}	0.97 ^{+0.02} _{-0.01}	79 ⁺²⁹ ₋₂₇	254 ⁺¹⁷ ₋₉	15 ⁺¹⁴¹ ₋₁₀₃	-89148 ⁺²⁵³¹ ₋₁₆₅₅	GE	*
NGC 7006	38.5	-144 ⁺⁵ ₋₄	-20 ⁺⁷ ₋₇	167 ⁺⁴ ₋₆	56.5 ^{+3.1} _{-3.2}	1.72 ^{+0.67} _{-0.48}	0.94 ^{+0.02} _{-0.02}	125 ⁺¹¹ ₋₁₀	758 ⁺⁵² ₋₅₄	-725 ⁺²⁴¹ ₋₂₄₉	-52150 ⁺¹⁷⁵⁹ ₋₁₉₅₆	GE	*
NGC 7078	10.6	6 ⁺⁵ ₋₇	119 ⁺⁶ ₋₆	123 ⁺⁶ ₋₆	10.6 ^{+0.4} _{-0.3}	3.60 ^{+0.29} _{-0.26}	0.49 ^{+0.03} _{-0.02}	28 ⁺² ₋₁	142 ⁺⁴ ₋₆	1128 ⁺⁷⁰ ₋₆₉	-119827 ⁺¹⁹¹⁹ ₋₁₇₈₉	D	
NGC 7089	10.4	168 ⁺⁵ ₋₅	-15 ⁺⁸ ₋₅	240 ⁺⁹ ₋₆	18.5 ^{+1.2} _{-0.9}	0.55 ^{+0.04} _{-0.24}	0.94 ^{+0.03} _{-0.00}	116 ⁺⁹ ₋₁₃	208 ⁺¹⁶ ₋₄₁	-120 ⁺⁶¹ ₋₁₁	-98441 ⁺³⁰³³ ₋₂₄₇₈	GE	
NGC 7099	7.2	-34 ⁺⁹ ₋₈	-55 ⁺¹² ₋₁₀	127 ⁺⁷ ₋₆	8.2 ^{+0.4} _{-0.2}	0.98 ^{+0.24} _{-0.29}	0.79 ^{+0.04} _{-0.05}	119 ⁺³ ₋₅	94 ⁺⁵ ₋₃	-233 ⁺⁵⁴ ₋₄₅	-137334 ⁺²⁴³⁷ ₋₁₇₉₀	GE	
Pal 12	15.7	143 ⁺²⁰ ₋₂₈	304 ⁺¹⁷ ₋₁₆	354 ⁺¹⁴ ₋₁₄	69.9 ^{+18.2} _{-14.3}	15.49 ^{+0.72} _{-0.55}	0.64 ^{+0.05} _{-0.06}	67 ⁺¹ ₋₂	1140 ⁺²⁹⁷ ₋₃₁₃	2142 ⁺¹⁴⁴ ₋₁₄₅	-42546 ⁺⁵⁰⁰⁸ ₋₅₂₀₂	Sgr	
Pal 13	27.0	264 ⁺⁵ ₋₅	-92 ⁺¹⁰ ₋₁₁	293 ⁺⁷ ₋₆	90.9 ^{+8.3} _{-7.2}	8.31 ^{+0.93} _{-0.64}	0.83 ^{+0.01} _{-0.01}	120 ⁺⁴ ₋₄	1418 ⁺¹⁶⁴ ₋₁₃₈	-1876 ⁺²³⁸ ₋₂₅₈	-37614 ⁺²¹⁴² ₋₂₀₉₇	GE	
NGC 7492	25.4	-91 ⁺¹⁸ ₋₁₃	-6 ⁺⁶ ₋₅	112 ⁺¹¹ ₋₁₄	28.3 ^{+3.3} _{-2.6}	3.34 ^{+1.20} _{-1.05}	0.79 ^{+0.06} _{-0.06}	92 ⁺² ₋₃	354 ⁺²⁹ ₋₂₂	-57 ⁺⁵⁹ ₋₄₅	-76660 ⁺²⁶³⁶ ₋₂₄₃₆	GE	*